Interplay of quark and meson degrees of freedom in near-threshold states: A practical parametrization for line shapes

F.-K. Guo,[1,2] C. Hanhart,[3] Yu. S. Kalashnikova,[4] P. Matuschek,[3] R. V. Mizuk,[5,6,7] A. V. Nefediev,[4,6,7] Q. Wang,[2,3] and J.-L. Wynen[3]

[1]*State Key Laboratory of Theoretical Physics, Institute of Theoretical Physics, Chinese Academy of Sciences, Beijing 100190, China*
[2]*Helmholtz-Institut für Strahlen- und Kernphysik and Bethe Center for Theoretical Physics, Universität Bonn, D-53115 Bonn, Germany*
[3]*Forschungszentrum Jülich, Institute for Advanced Simulation, Institut für Kernphysik (Theorie) and Jülich Center for Hadron Physics, D-52425 Jülich, Germany*
[4]*Institute for Theoretical and Experimental Physics, B. Cheremushkinskaya 25, Moscow 117218, Russia*
[5]*Lebedev Physics Institute, Leninsky Prospect 53, Moscow 119991, Russia*
[6]*National Research Nuclear University MEPhI, Kashirskoe Highway 31, Moscow 115409, Russia*
[7]*Moscow Institute of Physics and Technology, 9 Institutsky Lane, Dolgoprudny, Moscow Region 141700, Russia*

(Received 7 February 2016; published 22 April 2016)

We propose a practical parametrization for the line shapes of near-threshold states compatible with all requirements of unitarity and analyticity. The coupled-channel system underlying the proposed parametrization includes bare poles and an arbitrary number of elastic and inelastic channels treated fully nonperturbatively. The resulting formulas are general enough to be used for a simultaneous analysis of the data in all available production and decay channels of the (system of) state(s) under consideration for a quite wide class of reactions. As an example, we fit the experimental data currently available for several decay channels for the charged $Z_b^{(\prime)}$ states in the spectrum of bottomonia and find a good overall description of the data. We find the present data to be consistent with the $Z_b(10610)$ as a virtual state and with the $Z_b(10650)$ as a resonance, both residing very close to the $B\bar{B}^*$ and $B^*\bar{B}^*$ threshold, respectively.

DOI: 10.1103/PhysRevD.93.074031

I. INTRODUCTION

In the last decades an enormous bulk of data on the charmonia(like) and bottomonia(like) states lying above the open-flavor thresholds have been collected by many experiments, such as *BABAR*, Belle, BESIII, CDF, DØ, and LHCb. Future high luminosity experiments, in particular, the forthcoming experiment Belle-II at KEK and PANDA at FAIR, are expected to provide new high precision and high statistics data for already known states, as well as for new, yet unobserved ones in various final states [1–6]. Traditionally data in different channels were analyzed individually by use of Breit-Wigner distributions, or sums thereof, combined with some background function. However, this procedure provides only limited information on the state studied: first of all, Breit-Wigner parameters are reaction dependent; second, summing Breit-Wigners in general violates unitarity, and last but not least, by studying individual channels only, one does not exploit the full information content provided by the measurements. In particular, the theoretical description of the states above the open-flavor thresholds calls for using adequate parametrizations for the line shapes which should be capable of describing such phenomena as finite widths of the constituents, multiple thresholds in the vicinity of the resonances, an interplay of the quark and hadron degrees of freedom in near-threshold states, and so on. In the meantime, such parametrizations need to be easy to handle in order to be useful for the analysis of experimental data.

Consider first an unstable particle coupled to the hadronic channel, open at $E = 0$, with the coupling constant g_f. In the effective range approximation the scattering amplitude can be written in the form [7]

$$\mathcal{M}(E) = \frac{g_f/2}{E - E_0 + i(g_f/2)k}, \tag{1}$$

where the momentum k is

$$k(E) = \sqrt{2\mu E}\Theta(E) + i\sqrt{-2\mu E}\Theta(-E),$$

and μ is the reduced mass in the hadronic channel. Equation (1) can be viewed as the Breit-Wigner amplitude with the momentum dependence of the elastic width taken into account explicitly and it is valid, if the nearest additional threshold, located at $E = \Delta$, is far away from the considered threshold at $E = 0$, that is $|\Delta| \gg |E_0|$. Also, the direct interaction in the hadronic channel should not generate additional near-threshold poles in the S-matrix. As soon as one of these conditions fails Eq. (1) has to be generalized. In particular, in Ref. [8] such a generalization

is given for the case when the direct interaction in the hadronic channel does generate near-threshold poles in the S-matrix and a nontrivial interplay between quark and meson degrees of freedom takes place. The resulting line shapes may have quite a peculiar form, drastically different from the ones given by the simple Flatté formula of Eq. (1).

Straightforward generalizations of Eq. (1) to the multichannel case are discussed in Refs. [9–14], where all effects of the direct interaction between mesonic channels are absorbed into the effective coupling constants. More sophisticated approaches to the direct interactions in the mesonic channels are employed in Refs. [15,16]. Effects of the finite width of the constituents are discussed in Refs. [10,12,17]. Related discussions can also be found in Ref. [18].

In this paper we further extend the basis of states involved and consider a coupled-channel problem for near-threshold phenomena in a physical system which contains not only near-threshold poles and allows for additional elastic (in the example below, nearby open-flavor) mesonic channels, but also incorporates inelastic (in the example below, more distant hidden-flavor) channels fully nonperturbatively as required by unitarity. The resulting system of equations is expected to be rich enough to provide a realistic description of the line shapes for a quite wide class of reactions.

The formalism used is set up in a very general way. In particular, we allow for the inclusion of a set of "bare" poles in addition to various nonperturbative rescatterings. Effectively this provides an additional momentum- and energy-dependent interaction and therefore gives an additional flexibility for the fitting of experimental data, but does not *a priori* impose any assumption on the nature/wave function decomposition of a given state. In particular, with the pole terms included it becomes easily possible to also analyze systems with resonances above the thresholds. The main ideas as well as the key results have already been presented in Ref. [19]—here much more detailed derivations and discussions are presented and the updated experimental data are analyzed. In addition, we briefly discuss the possible role of the one-pion exchange.

For illustration of the formalism below we study decays of a system that contains a $\bar{Q}Q$ pair, with Q denoting a heavy quark. We refer to the open-flavor channels $(\bar{q}Q)(\bar{Q}q)$ (here q denotes a light quark) by greek letters α, β, … and to the hidden-flavor channels $(\bar{Q}Q)(\bar{q}q)$ by latin letters $i, j, \ldots$. The explicit poles are included as additional channels labeled by latin letters from the beginning of the alphabet, that is $a, b, \ldots$.

Paradigmatic examples of such physical systems are, e.g., the $X(3872)$ decaying into the open-charm channels $D\bar{D}^*$ [20] and the hidden-charm channels $\pi^+\pi^- J/\psi$ [21] and $\pi^+\pi^-\pi^0 J/\psi$ [22], or $Z_b(10610)$ and $Z_b(10650)$ decaying into the $B^{(*)}\bar{B}^*$ open-bottom [23] and $\pi\Upsilon(nS)/\pi h_b(mP)$ ($n = 1, 2, 3$, $m = 1, 2$) hidden-bottom [24] channels. While additional effects such as finite widths of the constituents and additional interactions between outgoing particles may also play a role and thus may have to be included on top of the interactions considered in this work (for a recent discussion of such effects see Ref. [25]), nevertheless the gross features of the coupled-channel problem are captured by the presented formalism and the parametrization based on it is expected to be realistic.

II. SOLUTION OF THE LIPPMANN-SCHWINGER EQUATION

A. Simplification of the Lippmann-Schwinger equation in a two-channel toy model

For the case of the structures near the open-flavor thresholds, as we will show, the coupled-channel Lippmann-Schwinger equation (LSE) can be simplified by absorbing some channels into the definition of an effective potential. To see how this works, it is instructive to study a simple two-channel toy model. In this subsection, we write the LSE in the operator form for simplicity. It will be written more explicitly in the form of integral equations in the next subsection.

Let us start with the LSE for the t matrix

$$t = v - vSt, \tag{2}$$

where S is the matrix for the free Green's functions in the channel space. The potential is parametrized as

$$v = \begin{pmatrix} v_{11} & v_{12} \\ v_{21} & v_{22} \end{pmatrix}. \tag{3}$$

Note that time reversal invariance demands that $v_{12} = v_{21}$ while for t to be unitary, all v_{ij}'s must be real. Explicitly, we have a system of four coupled-channel equations

$$t_{ij} = v_{ij} - \sum_{k=1,2} v_{ik} S_k t_{kj}, \qquad i, j = 1, 2, \tag{4}$$

which, however, effectively reduce to single-channel equations if any of the potentials v_{ij} vanishes. The two channels decouple from each other trivially if the off-diagonal components are set to zero, $v_{12} = v_{21} = 0$. Let us now focus on the case of a vanishing diagonal matrix element of v. For definiteness, we set $v_{22} = 0$. Then the t matrix components t_{12}, t_{21}, and t_{22} can be expressed through the component t_{11} straightforwardly,

$$\begin{aligned} t_{12} &= v_{12} - t_{11} S_1 v_{12}, \\ t_{21} &= v_{21} - v_{21} S_1 t_{11}, \\ t_{22} &= -v_{21} S_1 v_{12} + v_{21} S_1 t_{11} S_1 v_{12}, \end{aligned} \tag{5}$$

while t_{11} comes as a solution of a single-channel LSE

$$t_{11} = V_{11} - t_{11} S_1 V_{11} = V_{11} - V_{11} S_1 t_{11}, \tag{6}$$

with the effective potential

$$V_{11} = v_{11} - v_{12} S_2 v_{21}, \tag{7}$$

which admits a transparent physical interpretation: elastic scattering in channel 1 proceeds either through the direct interaction potential v_{11} or due to the transition through channel 2.

One sees therefore that channel 2 only enters additively in the effective potential, generalization to additional channels being trivial. This simplification can be applied to the case studied here because the interaction between a light hadron and a heavy quarkonium is Okubo-Zweig-Iizuka (OZI) forbidden and therefore it is very weak. We discuss a realistic case in the following sections.

B. Solution of the multichannel Lippmann-Schwinger equation

In this subsection we formulate a multichannel model and solve the corresponding Lippmann-Schwinger equations using the simplifying trick described in the previous subsection.

The key ingredients of the model are (i) the direct interaction in the open-flavor channels described by the potential $v_{\alpha\beta}(\boldsymbol{p},\boldsymbol{p}')$ as well as that in the hidden-flavor channels $v_{ij}(\boldsymbol{k},\boldsymbol{k}')$, (ii) the transition form factor between the open-flavor and hidden-flavor channels[1]

$$v_{\alpha i}(\boldsymbol{p},\boldsymbol{k}), \qquad \alpha = \overline{1, N_\mathrm{e}}, \qquad i = \overline{1, N_\mathrm{in}}, \tag{8}$$

and, finally, (iii) the transition form factors between the bare pole terms and the open-flavor and hidden-flavor channels,

$$v_{a\alpha}(\boldsymbol{p}) \quad \text{and} \quad v_{ai}(\boldsymbol{k}), \qquad a = \overline{1, N_\mathrm{p}}, \tag{9}$$

respectively. The open-flavor and hidden-flavor channels will alternatively be called elastic and inelastic channels, respectively. Note that unitarity in combination with the T-invariance calls for a real and symmetric scattering potential, as long as all relevant channels are included explicitly in the model. Actually, one can reverse this statement: if a high-quality fit for the data demands that some of the parameters be complex, the model should be regarded as incomplete. Thus, the formalism outlined here implicitly provides a diagnostic tool to investigate, whether or not for certain states all relevant channels are already discovered/included.

[1]A microscopic model for this interaction can be found, for example, in Refs. [26,27].

The interaction potential can be summarized in the form

$$\hat{V} = \begin{array}{c} \begin{matrix} b = \overline{1, N_\mathrm{p}} & \beta = \overline{1, N_\mathrm{e}} & i = \overline{1, N_\mathrm{in}} \end{matrix} \\ \begin{pmatrix} v_{ab} & v_{a\beta}(\boldsymbol{p}') & v_{ai}(\boldsymbol{k}) \\ v_{\alpha b}(\boldsymbol{p}) & v_{\alpha\beta}(\boldsymbol{p},\boldsymbol{p}') & v_{\alpha i}(\boldsymbol{p},\boldsymbol{k}) \\ v_{jb}(\boldsymbol{k}') & v_{j\beta}(\boldsymbol{k}',\boldsymbol{p}') & v_{ji}(\boldsymbol{k}',\boldsymbol{k}) \end{pmatrix} \end{array} \begin{array}{l} a = \overline{1, N_\mathrm{p}} \\ \alpha = \overline{1, N_\mathrm{e}} \\ j = \overline{1, N_\mathrm{in}} \end{array} \tag{10}$$

To simplify the notation we use the same symbol for incoming and outgoing vertex functions—however, the context will always make it clear which one is meant in a given equation. The number of the elastic channels N_e and the number of the inelastic channels N_in remain unspecified and can be chosen as large as suggested by the particular reaction being analyzed. For generality, we do not specify the number of bare poles either. The coupled channel problem with interaction potential (10) can be solved analytically, if a separable form of the transition form factors $v_{\alpha i}(\boldsymbol{p},\boldsymbol{k})$ is assumed. However such a general solution appears to be bulky and practically useless for the data analysis, since it requires multiple inversions of large matrices of the dimension $(N_\mathrm{e} + N_\mathrm{in} + N_\mathrm{p}) \times (N_\mathrm{e} + N_\mathrm{in} + N_\mathrm{p})$. Besides, inclusion of an additional inelastic channel requires the entire procedure to be started from scratch. Meanwhile, there are good reasons to neglect the direct interactions in the inelastic channels. For example, for the systems we focus on here such interactions are expected to be very weak—since there are no light quarks in heavy quarkonia, the interaction of pions with them is OZI suppressed and it thus vanishes at leading order in a low-energy expansion for the pion-quarkonium interaction. This conjecture is confirmed by the small values of the π-$\bar{Q}Q$ scattering lengths, which are estimated to be $\lesssim 0.02$ fm [28] and found to be consistent with 0 in lattice QCD studies [29,30]. Therefore, in the following we set $v_{ij}(\boldsymbol{k},\boldsymbol{k}') \equiv 0$. As a result, the interaction potential of Eq. (10) reads

$$\hat{V} = \begin{array}{c} \begin{matrix} B = \overline{1, N_\mathrm{e} + N_\mathrm{p}} & i = \overline{1, N_\mathrm{in}} \end{matrix} \\ \begin{pmatrix} v_{AB}(\boldsymbol{p},\boldsymbol{p}') & v_{Ai}(\boldsymbol{p},\boldsymbol{k}) \\ v_{jB}(\boldsymbol{k}',\boldsymbol{p}') & 0 \end{pmatrix} \end{array} \begin{array}{l} A = \overline{1, N_\mathrm{e} + N_\mathrm{p}} \\ j = \overline{1, N_\mathrm{in}} \end{array} \tag{11}$$

where, for convenience, we formally treat the pole terms as additional elastic channels and use capital greek letters for the corresponding indices, which now take values from 1 to $N_\mathrm{e} + N_\mathrm{p}$.

The toy model from the previous subsection tells us that omission of rescatterings within the inelastic channels introduces a great simplification since they enter only additively in the effective potential. Besides that we can completely disentangle elastic channels (including the pole terms) and inelastic channels. Consequently, solving the coupled-channel Lippmann-Schwinger equation amounts to the inversion of matrices as small as $(N_\mathrm{e} + N_\mathrm{p}) \times (N_\mathrm{e} + N_\mathrm{p})$ independent of the number of inelastic channels—see

Eq. (17). Furthermore, the formulas to be derived below allow one to disentangle the elastic channels from the bare poles too—see Eqs. (39), (41), (42)—so that eventually the problem reduces to inverting matrices as small as only $N_e \times N_e$ and $N_p \times N_p$ independently. For N_e and N_p smaller or equal to two, as in the case below, this can be done straightforwardly in the explicit form. Therefore the suggested approach guarantees a crucial simplification of the calculations. In particular, it speeds up the codes drastically, making combined analyses of experimental data in various channels significantly easier. Especially, adding an extra inelastic channel (explicitly or implicitly, through an additional constant inelasticity) changes the final expressions only marginally.

In order to formulate and solve the Lippmann-Schwinger equation for the scattering t matrix let us introduce the effective interaction potential in the elastic channels [cf. Eq. (7)]

$$V_{AB}(\boldsymbol{p},\boldsymbol{p}') = v_{AB}(\boldsymbol{p},\boldsymbol{p}') - \sum_i \int v_{Ai}(\boldsymbol{p},\boldsymbol{q}) S_i(\boldsymbol{q}) v_{iB}(\boldsymbol{q},\boldsymbol{p}') d^3q, \tag{12}$$

where the quantity $S_i(\boldsymbol{q})$ denotes the propagator of the ith $(\bar{Q}Q)(\bar{q}q)$ pair. The physical interpretation of this potential is straightforward: a transition from elastic channel A to elastic channel B proceeds either through the direct interaction potential $v_{AB}(\boldsymbol{p},\boldsymbol{p}')$ (including the pole terms) or through the inelastic channels, where the sum in i runs over all inelastic "bubbles." Notice that Eq. (12) as well as similar formulas below which contain capital Greek subscripts should be treated as schematic since, depending on a particular component of the corresponding potential or of the t matrix, the number of the arguments can be different—see Eq. (10). When written in components, potential (12) takes the form

$V_{ab} =$ 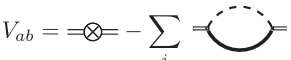

$$\begin{aligned} &= v_{ab} - \sum_i \int v_{ai}(\boldsymbol{q}) S_i(\boldsymbol{q}) v_{ib}(\boldsymbol{q}) d^3q \\ &\equiv -\mathcal{G}^{\rm in}_{0,ab}, \end{aligned} \tag{13}$$

$V_{\alpha a}(\boldsymbol{p}) =$ 

$$= v_{\alpha a}(\boldsymbol{p}) - \sum_i \int v_{\alpha i}(\boldsymbol{p},\boldsymbol{q}) S_i(\boldsymbol{q}) v_{ia}(\boldsymbol{q}) d^3q, \tag{14}$$

$V_{a\beta}(\boldsymbol{p}) =$ 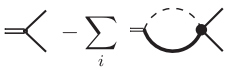

$$= v_{a\beta}(\boldsymbol{p}) - \sum_i \int v_{ai}(\boldsymbol{q}) S_i(\boldsymbol{q}) v_{i\beta}(\boldsymbol{q},\boldsymbol{p}) d^3q, \tag{15}$$

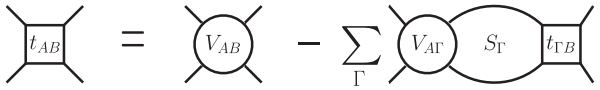

FIG. 1. Graphical representation of the Lippmann-Schwinger equation for the elastic scattering t matrix t_{AB}—see Eq. (17).

$V_{\alpha\beta}(\boldsymbol{p},\boldsymbol{p}') =$ 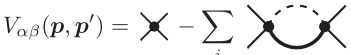

$$= v_{\alpha\beta}(\boldsymbol{p},\boldsymbol{p}') - \sum_i \int v_{\alpha i}(\boldsymbol{p},\boldsymbol{q}) S_i(\boldsymbol{q}) v_{i\beta}(\boldsymbol{q},\boldsymbol{p}') d^3q, \tag{16}$$

where the single thin (double) lines indicate the coupling to the open-flavor channels (pole terms) while the dashed and thick solid lines indicate the propagation of the light $\bar{q}q$ and heavy $\bar{Q}Q$ state, respectively.

The Lippmann-Schwinger equation for the elastic t matrix t_{AB} then reads (see Fig. 1)

$$\begin{aligned} t_{AB}(\boldsymbol{p},\boldsymbol{p}') &= V_{AB}(\boldsymbol{p},\boldsymbol{p}') \\ &\quad - \sum_\Gamma \int V_{A\Gamma}(\boldsymbol{p},\boldsymbol{q}) S_\Gamma(\boldsymbol{q}) t_{\Gamma B}(\boldsymbol{q},\boldsymbol{p}') d^3q, \end{aligned} \tag{17}$$

where $S_\alpha(\boldsymbol{p})$ is the propagator of the α-th $(\bar{q}Q)(\bar{Q}q)$ pair, and

$$S_{0,aa} \equiv \int \mathcal{S}_a(\boldsymbol{q}) d^3q = \frac{1}{M_{0,a} - M - i0} \tag{18}$$

denotes the nonvanishing matrix elements of the diagonal matrix of the bare pole propagators with $M_{0,a}$ being the bare mass. Below the results for the elastic and inelastic loop integrals will be parametrized conveniently such that the explicit form of the propagators $S_i(\boldsymbol{q})$ and $S_\alpha(\boldsymbol{q})$ is of no relevance.

Once a solution of the Lippmann-Schwinger equation (17) for the elastic t matrix t_{AB} is found, all other components of

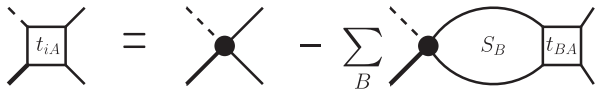

FIG. 2. Graphical representation of the expression for the t matrix component t_{iA} given in Eq. (21). Representation for the component t_{Ai} takes a similar form and it is not shown. The solid lines are for the heavy-light $(\bar{q}Q)$ and $(\bar{Q}q)$ mesons with open flavor, the fat solid line is for the hidden-flavor heavy meson $(\bar{Q}Q)$, and the dashed line is for the light meson $(\bar{q}q)$.

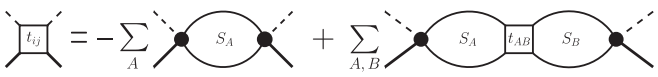

FIG. 3. Graphical representation of the expression for the t matrix component t_{ij} given in Eq. (21). For the lines' identification see the caption of Fig. 2.

the t matrix can be found algebraically, without having to solve further equations (see Figs. 2 and 3):

$$t_{Ai}(\boldsymbol{p},\boldsymbol{k}) = v_{Ai}(\boldsymbol{p},\boldsymbol{k}) - \sum_B \int t_{AB}(\boldsymbol{p},\boldsymbol{q}) S_B(\boldsymbol{q}) \times v_{Bi}(\boldsymbol{q},\boldsymbol{k}) d^3q, \tag{19}$$

$$t_{iA}(\boldsymbol{k},\boldsymbol{p}) = v_{iA}(\boldsymbol{k},\boldsymbol{p}) - \sum_B \int v_{iB}(\boldsymbol{k},\boldsymbol{q}) S_B(\boldsymbol{q}) t_{BA}(\boldsymbol{q},\boldsymbol{p}) d^3q, \tag{20}$$

$$\begin{aligned} t_{ij}(\boldsymbol{k},\boldsymbol{k}') = &-\sum_A \int v_{iA}(\boldsymbol{k},\boldsymbol{q}) S_A(\boldsymbol{q}) v_{Aj}(\boldsymbol{q},\boldsymbol{k}') d^3q \\ &+ \sum_{A,B} \int v_{iA}(\boldsymbol{k},\boldsymbol{q}) S_A(\boldsymbol{q}) t_{AB}(\boldsymbol{q},\boldsymbol{q}') S_B(\boldsymbol{q}') \\ &\times v_{Bj}(\boldsymbol{q}',\boldsymbol{k}') d^3q d^3q'. \end{aligned} \tag{21}$$

Equation (17) can be written explicitly for the t matrix components $t_{\alpha\beta}$, $t_{\alpha a}$, $t_{a\alpha}$, and t_{ab}, and it splits into two decoupled systems of equations. By simple algebraic transformations it is straightforward to exclude the components t_{ab} and $t_{a\alpha}$ to arrive at the following decoupled Lippmann-Schwinger equations for the elastic t matrix $t_{\alpha\beta}$,

$$t_{\alpha\beta}(\boldsymbol{p},\boldsymbol{p}') = V^{\rm eff}_{\alpha\beta}(\boldsymbol{p},\boldsymbol{p}') - \sum_\gamma \int V^{\rm eff}_{\alpha\gamma}(\boldsymbol{p},\boldsymbol{q}) S_\gamma(\boldsymbol{q}) t_{\gamma\beta}(\boldsymbol{q},\boldsymbol{p}') d^3q, \tag{22}$$

and for the component $t_{\alpha a}(\boldsymbol{p})$,

$$t_{\alpha a}(\boldsymbol{p}) = V^{\rm eff}_{\alpha a}(\boldsymbol{p}) - \sum_\beta \int V^{\rm eff}_{\alpha\beta}(\boldsymbol{p},\boldsymbol{q}) S_\beta(\boldsymbol{q}) t_{\beta a}(\boldsymbol{q}) d^3q. \tag{23}$$

The matrix for the pole propagators dressed by the inelastic channels reads

$$G_0 = (S_0^{-1} - \mathcal{G}_0^{\rm in})^{-1}, \tag{24}$$

where the inelastic loop matrix $\mathcal{G}_0^{\rm in}$ is defined in Eq. (13).

In the single-pole case ($a = 0$) G_0 is simply

$$G_0 = \frac{1}{M_0 - M + V_{00} - i0}. \tag{25}$$

The real part of $\mathcal{G}_0^{\rm in} = -V_{00}$ can be absorbed into the renormalization of the bare pole position M_0, while its imaginary part shifts the pole to the complex plane, away from the real axis. Note that the explicit form of $\mathcal{G}_0^{\rm in}$ links the imaginary part of the pole location to the corresponding transitions to the inelastic channels as demanded by unitarity.

For multiple bare poles the real parts of the diagonal elements $\mathcal{G}^{\rm in}_{0,aa}$ can also be absorbed by the bare masses

FIG. 4. The full effective interaction potential in the elastic channels—see Eq. (27). The double solid line is for the pole term propagator G_0 [see Eq. (24)] while for the other lines' identification see the caption of Fig. 2. Potentials $V_{\alpha a}$ and $V_{b\beta}$ are defined in Eqs. (14) and (15).

$M_{0,a}$—see Eq. (18)—while the off-diagonal elements $\mathcal{G}^{\rm in}_{0,ab}$ ($a \neq b$) describe the transition potentials between the bare states, and in general their real parts,

$$\kappa^{\rm in}_{ab} \equiv {\rm Re}(\mathcal{G}^{\rm in}_{0,ab}), \quad \text{for } a \neq b, \tag{26}$$

need to be retained as additional parameters of the model. For example, in the case of two bare poles there is one such additional parameter $\kappa^{\rm in}_{12} = \kappa^{\rm in}_{21}$.

The effective potential $V^{\rm eff}_{\alpha\beta}(\boldsymbol{p},\boldsymbol{p}')$ is depicted schematically in Fig. 4 and reads

$$\begin{aligned} V^{\rm eff}_{\alpha\beta}(\boldsymbol{p},\boldsymbol{p}') = &\, v_{\alpha\beta}(\boldsymbol{p},\boldsymbol{p}') - \sum_{a,b} V_{\alpha a}(\boldsymbol{p}) G_{0,ab} V_{b\beta}(\boldsymbol{p}') \\ &- \sum_i \int v_{\alpha i}(\boldsymbol{p},\boldsymbol{q}) S_i(\boldsymbol{q}) v_{i\beta}(\boldsymbol{q},\boldsymbol{p}') d^3q, \end{aligned} \tag{27}$$

while the effective potential $V^{\rm eff}_{\alpha a}$ is

$$V^{\rm eff}_{\alpha a}(\boldsymbol{p}) = (M_{0,a} - M) \sum_b V_{\alpha b}(\boldsymbol{p}) G_{0,ba}. \tag{28}$$

III. ANALYTIC SOLUTION FOR SEPARABLE INTERACTIONS

To proceed towards an analytic solution we assume the vertex in Eq. (8) to possess a separable form,

$$v_{\alpha i}(\boldsymbol{p},\boldsymbol{k}) = \chi_{i\alpha}(\boldsymbol{p}) \varphi_{i\alpha}(\boldsymbol{k}), \tag{29}$$

which is necessary to express all the t matrix elements in terms of those for the direct interaction, given by Eq. (36) below. It is obvious that the definition of Eq. (29) is invariant under the transformation

$$\chi_{i\alpha}(\boldsymbol{p}) \to C \chi_{i\alpha}(\boldsymbol{p}), \qquad \varphi_{i\alpha}(\boldsymbol{k}) \to \varphi_{i\alpha}(\boldsymbol{k})/C, \tag{30}$$

with an arbitrary, real constant C, so that without loss of generality one can set

$$\chi_{i\alpha}(\boldsymbol{p} = 0) = 1. \tag{31}$$

A considerable simplification of Eqs. (22) and (23) can be achieved if the form factor $\chi_{i\alpha}(\boldsymbol{p})$ entering vertex function (29) is assumed independent of the inelastic channel, that is

$$v_{\alpha i}(\boldsymbol{p},\boldsymbol{k}) = \chi_\alpha(\boldsymbol{p})\varphi_{i\alpha}(\boldsymbol{k}). \tag{32}$$

In fact, it is quite natural to assume that $\chi_{i\alpha}$ is independent of i, since the transition of the open-flavor channels to the hidden-flavor channels demands the exchange of a heavy meson and therefore it is of a short-range nature for all inelastic channels as long as these channels are far from the thresholds of the elastic channels (so that the exchanged heavy meson is far off shell). By virtue of Eq. (32) the effective potential defined in Eq. (27) reads

$$V^{\rm eff}_{\alpha\beta}(\boldsymbol{p},\boldsymbol{p}') = v_{\alpha\beta}(\boldsymbol{p},\boldsymbol{p}') - \chi_\alpha(\boldsymbol{p})G_{\alpha\beta}\chi_\beta(\boldsymbol{p}') - \sum_{a,b} V_{\alpha a}(\boldsymbol{p})G_{0,ab}V_{b\beta}(\boldsymbol{p}'), \tag{33}$$

where the inelastic bubble operator $G_{\alpha\beta}$ is

$$G_{\alpha\beta} \equiv \sum_i G^i_{\alpha\beta} = \sum_i \int \varphi_{\alpha i}(\boldsymbol{q})S_i(\boldsymbol{q})\varphi_{i\beta}(\boldsymbol{q})d^3q. \tag{34}$$

In order to solve Eqs. (22) and (23) we proceed stepwise. The strategy basically represents a successive application of the two-potential formalism [31] (see also Ref. [32] for an application to a physical system more closely related to the one of relevance here):

(1) In the first step only the direct interaction $v_{\alpha\beta}(\boldsymbol{p},\boldsymbol{p}')$ [the first term in potential (33)] is retained and a convenient parametrization is given for the corresponding direct interaction t matrix hereinafter denoted as t^v;
(2) then the coupling to the inelastic channels is switched on [the second term in potential (33)] and a scattering equation for the potential

$$w_{\alpha\beta}(\boldsymbol{p},\boldsymbol{p}') = v_{\alpha\beta}(\boldsymbol{p},\boldsymbol{p}') - \chi_\alpha(\boldsymbol{p})G_{\alpha\beta}\chi_\beta(\boldsymbol{p}') \tag{35}$$

is solved, with the solution denoted as t^w (notice that here the repeated indices do not imply a resummation which is always written explicitly in this paper);
(3) finally, the coupling to the pole terms [the last term in potential (33)] is included, in addition. The result provides the solution to the full problem defined in Eqs. (22) and (23).

We therefore start assuming that a solution t^v of the Lippmann-Schwinger equation

$$t^v_{\alpha\beta}(\boldsymbol{p},\boldsymbol{p}') = v_{\alpha\beta}(\boldsymbol{p},\boldsymbol{p}') - \sum_\gamma \int v_{\alpha\gamma}(\boldsymbol{p},\boldsymbol{q})S_\gamma(\boldsymbol{q})t^v_{\gamma\beta}(\boldsymbol{q},\boldsymbol{p}')d^3q \tag{36}$$

for the bare direct interaction $v_{\alpha\beta}(\boldsymbol{p},\boldsymbol{p}')$ is known. For instance, it can be simply parametrized in a convenient form—see Refs. [8,16] and the discussion in Sec. VI B below. This finalizes step 1 above.

As the coupling to the inelastic channels is switched on (step 2), the bare form factors $\chi_\alpha(\boldsymbol{p})$ get dressed by the elastic interactions. It is therefore convenient to define new incoming and outgoing form factors $\psi_{\alpha\beta}(\boldsymbol{p})$ and $\bar\psi_{\alpha\beta}(\boldsymbol{p})$, respectively, dressed with the direct interaction potential $v_{\alpha\beta}(\boldsymbol{p},\boldsymbol{p}')$,[2]

$\psi_{\alpha\beta}(\boldsymbol{p}) =$ 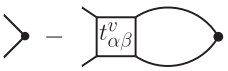

$$= \delta_{\alpha\beta}\chi_\alpha(\boldsymbol{p}) - \int t^v_{\alpha\beta}(\boldsymbol{p},\boldsymbol{q})S_\beta(\boldsymbol{q})\chi_\beta(\boldsymbol{q})d^3q, \tag{37}$$

$\bar\psi_{\alpha\beta}(\boldsymbol{p}) =$ 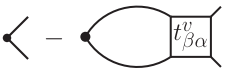

$$= \delta_{\alpha\beta}\chi_\alpha(\boldsymbol{p}) - \int \chi_\alpha(\boldsymbol{q})S_\alpha(\boldsymbol{q})t^v_{\alpha\beta}(\boldsymbol{q},\boldsymbol{p})d^3q. \tag{38}$$

It is straightforward now to find the solution of the Lippmann-Schwinger equation for the potential given in Eq. (35) in the form

$$t^w_{\alpha\beta}(\boldsymbol{p},\boldsymbol{p}') = t^v_{\alpha\beta}(\boldsymbol{p},\boldsymbol{p}') + \sum_{\gamma,\delta}\psi_{\alpha\gamma}(\boldsymbol{p})([\mathcal{G}-G^{-1}]^{-1})_{\gamma\delta}\bar\psi_{\delta\beta}(\boldsymbol{p}'), \tag{39}$$

where the matrix G is given in Eq. (34) while the matrix $\mathcal{G}$ is defined as

$\mathcal{G}_{\alpha\beta} =$  $= \int \chi_\alpha(\boldsymbol{q})S_\alpha(\boldsymbol{q})\psi_{\alpha\beta}(\boldsymbol{q})d^3q$

$=$  $= \int \bar\psi_{\alpha\beta}(\boldsymbol{q})S_\beta(\boldsymbol{q})\chi_\beta(\boldsymbol{q})d^3q.$ (40)

This finalizes step 2.

To accomplish the work program and to build solutions of Eqs. (22) and (23) we apply again the two-potential formalism to include the bare pole terms and to express the full t matrix elements in terms of t^w. This is a multipole generalization of the formulas derived in Ref. [16]. We find that

$$t_{\alpha\beta}(\boldsymbol{p},\boldsymbol{p}') = t^w_{\alpha\beta}(\boldsymbol{p},\boldsymbol{p}') + \sum_{a,b}\phi_{\alpha a}(\boldsymbol{p})(\mathcal{G}^{\rm e}_0 - G^{-1}_0)^{-1}_{ab}\bar\phi_{b\beta}(\boldsymbol{p}'), \tag{41}$$

[2]Notice that once the bare form factor $\chi_\alpha(\boldsymbol{p})$ does not depend on the inelastic channel, the dressed form factors $\psi_{\alpha\beta}(\boldsymbol{p})$ and $\bar\psi_{\alpha\beta}(\boldsymbol{p})$ do not depend on it either.

$$= t^w_{\alpha\beta}(\boldsymbol{p},\boldsymbol{p}') + \sum_{a,b}\phi_{aa}(\boldsymbol{p})(\mathcal{G}^{\rm e}_0 + \mathcal{G}^{\rm in}_0 - S_0^{-1})^{-1}_{ab}\bar{\phi}_{b\beta}(\boldsymbol{p}'),$$

$$t_{aa}(\boldsymbol{p}) = -\sum_b \phi_{ab}(\boldsymbol{p})[S_0(\mathcal{G}^{\rm e}_0 - G_0^{-1})]^{-1}_{ba}$$

$$= \sum_b \phi_{ab}(\boldsymbol{p})[1 - S_0(\mathcal{G}^{\rm e}_0 + \mathcal{G}^{\rm in}_0)]^{-1}_{ba}, \quad (42)$$

where Eq. (24) was used to find G_0^{-1}, and

$$\phi_{\alpha a}(\boldsymbol{p}) =$$

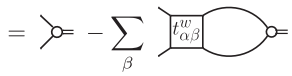

$$= V_{\alpha a}(\boldsymbol{p}) - \sum_\beta \int t^w_{\alpha\beta}(\boldsymbol{p},\boldsymbol{q})S_\beta(\boldsymbol{q})V_{\beta a}(\boldsymbol{q})d^3q, \quad (43)$$

$$\bar{\phi}_{a\alpha}(\boldsymbol{p}) =$$

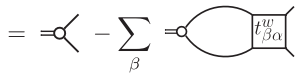

$$= V_{a\alpha}(\boldsymbol{p}) - \sum_\beta \int V_{a\beta}(\boldsymbol{q})S_\beta(\boldsymbol{q})t^w_{\beta\alpha}(\boldsymbol{q},\boldsymbol{p})d^3q, \quad (44)$$

$$\mathcal{G}^{\rm e}_{0,ab} =$$

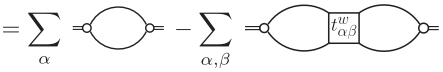

$$= \sum_\alpha \int V_{a\alpha}(\boldsymbol{q})S_\alpha(\boldsymbol{q})\phi_{\alpha b}(\boldsymbol{q})d^3q$$

$$= \sum_\alpha \int \bar{\phi}_{a\alpha}(\boldsymbol{q})S_\alpha(\boldsymbol{q})V_{\alpha b}(\boldsymbol{q})d^3q. \quad (45)$$

This finalizes step 3 and the entire work program.

Finally, the t matrix component $t_{\alpha i}$ can be found from the first equation in system (21),

$$t_{\alpha i}(\boldsymbol{p},\boldsymbol{k}) = v_{\alpha i}(\boldsymbol{p},\boldsymbol{k}) - \sum_a t_{aa}(\boldsymbol{p})S_{0,aa}v_{ai}(\boldsymbol{k}) - \sum_\beta \int t_{\alpha\beta}(\boldsymbol{p},\boldsymbol{q})S_\beta(\boldsymbol{q})v_{\beta i}(\boldsymbol{q},\boldsymbol{k})d^3q, \quad (46)$$

so that $t_{\alpha i}$ is fully determined through the t matrices $t_{\alpha\beta}$ and t_{aa} explicitly found above.

The remaining components of the full t matrix, namely t_{ab}, t_{aa}, $t_{i\alpha}$, and t_{ij}, will not be used in what follows and therefore are not quoted here explicitly.

IV. PRODUCTION AMPLITUDES AND RATES

There is no experimental possibility to study the elastic scattering of flavored mesons off each other, and our knowledge of the properties of near-threshold states comes from production experiments. For the production amplitudes one needs to add $N_{\rm e}$ sources for the elastic channels, $N_{\rm in}$ sources for the inelastic channels and $N_{\rm p}$ sources for the pole terms. It is sufficient to treat all sources as pointlike. On the other hand, when focusing on near-threshold phenomena it is natural to assume that the production proceeds predominantly through the elastic channels, so that it is sufficient to assume that only $N_{\rm e}$ elastic sources exist, with the strengths $\mathcal{F}_\alpha$. Therefore the production problem is set up as follows: (i) an elastic channel is produced from a pointlike source, accompanied by a spectator; (ii) for simplicity, the interaction in the final state between the spectator and the other particles is neglected (this assumption allows one to proceed with analytical calculations, but it can be relaxed in numerical computations); (iii) due to rescatterings, any elastic or inelastic channel x can be produced in the final state.

In Fig. 5 the contributions to the production amplitude in the channel x (elastic or inelastic) are presented in a graphical form, and the corresponding expression reads

$$\mathcal{M}^{\rm e}_\alpha(\boldsymbol{p}) = \mathcal{F}_\alpha(\boldsymbol{p}) - \sum_\beta \int \mathcal{F}_\beta(\boldsymbol{q})S_\beta(\boldsymbol{q})t_{\beta\alpha}(\boldsymbol{q},\boldsymbol{p})d^3q, \quad (47)$$

for the elastic channel $x = \alpha$, or

$$\mathcal{M}^{\rm in}_i(\boldsymbol{k}) = -\sum_\alpha \int \mathcal{F}_\alpha(\boldsymbol{q})S_\alpha(\boldsymbol{q})t_{\alpha i}(\boldsymbol{q},\boldsymbol{k})d^3q, \quad (48)$$

for the inelastic channel $x = i$.

To proceed with the calculations of the differential production rates we start from the standard expression for the differential decay width [33]

$$\frac{d\Gamma_x}{dm^2_{12}dm^2_{23}} = \frac{1}{(2\pi)^3}\frac{1}{32M^3_{\rm tot}}|\mathcal{M}_x|^2, \quad (49)$$

where $M_{\rm tot}$ is the total energy of the system. Since we neglect the final state interaction between the spectator (particle 3) and the rest of the system (particles 1 and 2) the integration in the invariant mass m^2_{23} is trivial and yields

$$\int_{(m^2_{23})_{\rm min}}^{(m^2_{23})_{\rm max}} dm^2_{23} = \frac{1}{m^2_{12}}\lambda^{1/2}(m^2_{12},m^2_1,m^2_2) \times \lambda^{1/2}(M^2_{\rm tot},m^2_{12},m^2_3) = \frac{4M_{\rm tot}}{m_{12}}k_{3(12)}k_{12}, \quad (50)$$

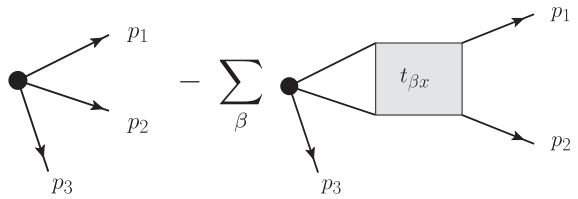

FIG. 5. Graphical representation of the contributions to the production amplitude for the channel x from a pointlike source: Born term (first diagram) and rescattering term (second diagram).

where $\lambda(x^2, y^2, z^2)$ is the standard triangle function while $k_{3(12)} \equiv p_3$ and $k_{12} \equiv k_x$ are the 3-momentum of particle 3 in the center-of-mass frame of particles 1 and 2, and the 3-momentum of particles 1 and 2 in the rest frame of the decaying particle, respectively. Then for the differential rate $d\mathrm{Br}_x \equiv d\Gamma_x/\Gamma_{\mathrm{tot}}$ we get

$$\frac{d\mathrm{Br}_x}{ds} = \frac{|\mathcal{M}_x|^2 p_3 k_x}{64\pi^3 M_{\mathrm{tot}}^2 \Gamma_{\mathrm{tot}} \sqrt{s}}, \tag{51}$$

where $s \equiv M^2 = m_{12}^2$ and, consequently,

$$\frac{d\mathrm{Br}_x}{dM} = \frac{|\mathcal{M}_x|^2 p_3 k_x}{32\pi^3 M_{\mathrm{tot}}^2 \Gamma_{\mathrm{tot}}}. \tag{52}$$

Finally, the total rate comes as an integral,

$$\mathrm{Br}_x = \int_{M_{\mathrm{min}}}^{M_{\mathrm{max}}} \left(\frac{d\mathrm{Br}_x}{dM}\right) dM, \tag{53}$$

where $M_{\mathrm{min}} = m_1 + m_2$ and $M_{\mathrm{max}} = M_{\mathrm{tot}} - m_3$.

V. TOWARDS A CONVENIENT PARAMETRIZATION OF THE LINE SHAPES

The expressions for the t matrix components and for the rates derived above can be used to build a sufficiently general parametrization applicable for the description of a wide class of near-threshold phenomena.

In the near-threshold region and for S-wave coupling of the elastic channels, the vertex form factors $\chi_\alpha(\boldsymbol{p})$ can be approximated by constants $\chi_\alpha(0)$ which, by virtue of the normalization condition (31), are simply equal to unity. Thus, the integrals entering Eqs. (37), (38), and (40) can be evaluated as

$$\begin{aligned} \int \chi_\alpha^2(\boldsymbol{q}) S_\alpha(\boldsymbol{q}) d^3q &\approx \chi_\alpha^2(0) J_\alpha = J_\alpha, \\ \int \chi_\alpha(\boldsymbol{q}) S_\alpha(\boldsymbol{q}) d^3q &\approx \chi_\alpha(0) J_\alpha = J_\alpha, \end{aligned} \tag{54}$$

where the nonrelativistic loop integral is

$$J_\alpha = \int S_\alpha(\boldsymbol{p}) d^3p = (2\pi)^2 \mu_\alpha(\kappa_\alpha + ik_\alpha) \equiv R_\alpha + iI_\alpha, \tag{55}$$

with μ_α and k_α being the reduced mass and the momentum in the α's elastic channel, respectively.

Then one arrives at the expressions

$$\begin{aligned} \psi_{\alpha\beta} &= \delta_{\alpha\beta} - t^v_{\alpha\beta} J_\beta, \\ \bar{\psi}_{\alpha\beta} &= \delta_{\alpha\beta} - J_\alpha t^v_{\alpha\beta}, \\ \mathcal{G}_{\alpha\beta} &= \delta_{\alpha\beta} J_\alpha - J_\alpha t^v_{\alpha\beta} J_\beta \end{aligned} \tag{56}$$

for the dressed form factors (38) and for matrix (40), respectively.

According to Eqs. (13), (26) and (34) the contribution of the inelastic channels is given by

$$\begin{aligned} \mathcal{G}^{\mathrm{in}}_{0,ab} &= -v_{ab} + \sum_i \int v_{ai}(\boldsymbol{q}) S_i(\boldsymbol{q}) v_{ib}(\boldsymbol{q}) d^3q \\ &\to \kappa^{\mathrm{in}}_{ab} + \frac{i(2\pi)^2}{\sqrt{s}} \sum_i m_{\mathrm{th}^{\mathrm{in}}_i} \mu^{\mathrm{in}}_i \lambda_{ai} \lambda_{bi} (k^{\mathrm{in}}_i)^{2l_i+1}, \end{aligned} \tag{57}$$

where $\kappa^{\mathrm{in}}_{ab}$ has only off-diagonal elements (see the explanation below), and by

$$\begin{aligned} G_{\alpha\beta} &= \sum_i \int \varphi_{i\alpha}(\boldsymbol{q}) S_i(\boldsymbol{q}) \varphi_{i\beta}(\boldsymbol{q}) d^3q \\ &\to \frac{i(2\pi)^2}{\sqrt{s}} \sum_i m_{\mathrm{th}^{\mathrm{in}}_i} \mu^{\mathrm{in}}_i g_{i\alpha} g_{i\beta} (k^{\mathrm{in}}_i)^{2l_i+1}, \end{aligned} \tag{58}$$

where the transition form factors were written in the form

$$v_{ai}(\boldsymbol{k}) = v_{ia}(\boldsymbol{k}) = \lambda_{ai} |\boldsymbol{k}|^{l_i}, \qquad \varphi_{i\alpha}(\boldsymbol{k}) = g_{i\alpha} |\boldsymbol{k}|^{l_i}, \tag{59}$$

while l_i, μ^{in}_i, and k^{in}_i are the angular momentum, the reduced mass, and the momentum in the ith inelastic channel, respectively, and $m_{\mathrm{th}^{\mathrm{in}}_i}$ is the corresponding threshold.

In Eq. (57) the constant real parts $\kappa^{\mathrm{in}}_{ab}$ include both the mixing among bare poles v_{ab} and the real parts of the inelastic loops—see Eqs. (26) and (13). The diagonal elements $\kappa^{\mathrm{in}}_{aa}$ should be set to zero since they only renormalize the bare pole positions $M_{0,a}$—see the discussion above Eq. (26).

Similarly, in Eq. (58) the constant part of $G_{\alpha\beta}$ was omitted since it renormalizes parameters of the direct interaction potential $v_{\alpha\beta}$—see Eq. (33). Equations (57) and (58) provide a natural generalization of the K-matrix approach. Notice however that in a typical situation inelastic thresholds reside sufficiently far below the elastic ones, so that near the elastic thresholds, neither analyticity nor unitarity are violated by using the truncated expressions for $\mathcal{G}^{\mathrm{in}}_0$ and $G_{\alpha\beta}$. As was already mentioned above, in the presented model the inelastic channels enter additively, so that an extension of the model to include an extra inelastic channel is straightforward [see Eqs. (57) and (58)] and does not enlarge the matrices that need to be inverted to solve the scattering problem. In the case of only remote inelastic channels the dependence of the momenta k^{in}_i on the energy can be neglected. Therefore, if the open inelastic thresholds reside far away from the energy region of interest (in particular, far from the elastic thresholds), their contribution can be mimicked by simply giving the bare pole positions $M_{0,a}$ as well as the direct interaction potentials v_{ab} and $v_{\alpha\beta}$ a constant imaginary part.

It is straightforward now to build the t matrix t^w given by Eq. (39) as

$$t^w(M) = t^v(M) + \psi[\mathcal{G} - G^{-1}]^{-1}\bar{\psi}. \tag{60}$$

If the bare pole terms are present in the system then, similarly to Eq. (54), one can write

$$\int v_{a\alpha}(\boldsymbol{q}) S_\alpha(\boldsymbol{q}) v_{\alpha b}(\boldsymbol{q}) d^3q \approx v_{a\alpha} v_{b\alpha} J_\alpha,$$
$$\int v_{a\alpha}(\boldsymbol{q}) S_\alpha(\boldsymbol{q}) d^3q \approx v_{a\alpha} J_\alpha, \tag{61}$$

where $v_{a\alpha} = v_{a\alpha}(0) = v_{\alpha a}(0)$, and

$$V_{\alpha a} = V_{a\alpha} = v_{a\alpha} - \frac{i(2\pi)^2}{\sqrt{s}} \sum_i m_{\mathrm{th}_i^{\mathrm{in}}} \mu_i^{\mathrm{in}} g_{i\alpha} \lambda_{ai} (k_i^{\mathrm{in}})^{2l_i+1}, \tag{62}$$

where, as before, the energy-independent parts of the sums were absorbed into the renormalization of the constants $v_{a\alpha}$.

Then quantities $\phi_{\alpha a}$, $\bar{\phi}_{a\alpha}$ and $\mathcal{G}^{\mathrm{e}}_{0,ab}$ defined in Eqs. (43), (44), and (45) can be built as

$$\phi_{\alpha a} = V_{\alpha a} - \sum_\beta t^w_{\alpha\beta} J_\beta V_{\beta a},$$
$$\bar{\phi}_{a\alpha} = V_{a\alpha} - \sum_\beta V_{a\beta} J_\beta t^w_{\beta\alpha},$$
$$\mathcal{G}^{\mathrm{e}}_{0,ab} = \sum_\alpha V_{a\alpha} J_\alpha V_{\alpha b} - \sum_{\alpha,\beta} V_{a\alpha} J_\alpha t^w_{\alpha\beta} J_\beta V_{\beta b}, \tag{63}$$

respectively, which when substituted into Eqs. (41), (42) and (46) allow one to find the expressions for $t_{\alpha\beta}$, $t_{\alpha a}$ and t_{ai} in their ultimate form.

Then for the αth elastic channel in the final state and for constant sources $\mathcal{F}_\alpha$ production amplitude (47) is

$$\mathcal{M}^{\mathrm{e}}_\alpha = \mathcal{F}_\alpha - \sum_\beta \int \mathcal{F}_\beta S_\beta(\boldsymbol{q}) t_{\beta\alpha} d^3q$$
$$= \mathcal{F}_\alpha - \sum_\beta \mathcal{F}_\beta J_\beta t_{\beta\alpha}. \tag{64}$$

If the t matrix has near-threshold poles, then the Born term can be neglected, provided that we focus on the near-threshold region (a detailed discussion can be found in Ref. [8]). Strictly speaking, neglecting the Born term violates unitarity; however this violation is negligibly small and it is controlled by the proximity of the t matrix poles to the threshold(s).[3]

Similarly, for the ith inelastic channel in the final state we have [see Eq. (48)]

$$\mathcal{M}^{\mathrm{in}}_i = -\sum_\alpha \mathcal{F}_\alpha J_\alpha t_{\alpha i}. \tag{65}$$

Accordingly the expressions for the differential production rates are

$$\frac{d\mathrm{Br}_\alpha}{dM} = \left| \sum_\beta \mathcal{F}_\beta t_{\beta\alpha} \right|^2 p_3 k_\alpha \tag{66}$$

and

$$\frac{d\mathrm{Br}_i}{dM} = \left| \sum_\alpha \mathcal{F}_\alpha t_{\alpha i} \right|^2 p_3 k_i^{\mathrm{in}}, \tag{67}$$

where the source terms $\mathcal{F}_\alpha$ were redefined to absorb the slowly varying function of energy $J_\alpha = R_\alpha + iI_\alpha \approx R_\alpha$ as well as all constant factors from Eq. (52).

To simplify notations and to make the physical meaning of the parameters more transparent we define

$$\mathcal{N} = \mathcal{F}_1^2, \qquad \xi_\alpha = \mathcal{F}_\alpha / \mathcal{F}_1. \tag{68}$$

In addition, since for all elastic channels the range of forces is described by the same physics, it is natural to set $\kappa_\alpha = \kappa$ in all R_α's [see Eq. (55)].

Therefore, the line shapes for the production in N_{e} elastic and N_{in} inelastic channels are described by the following set of parameters:

$$\mathcal{N},\ \xi_\alpha,\ v_{a\alpha},\ \lambda_{ai},\ g_{i\alpha},\ M_{0,a},\ \kappa,\ \kappa^{\mathrm{in}}_{ab}(a \neq b),\ t^v, \tag{69}$$

that is by $N_{\mathrm{v}} + N_{\mathrm{in}}(N_{\mathrm{e}} + N_{\mathrm{p}}) + (N_{\mathrm{p}} + 1)(N_{\mathrm{e}} + 1) + N_{\mathrm{p}}(N_{\mathrm{p}} - 1)/2 + 1$ real parameters (N_{v} is the number of parameters for the direct interaction t matrix t^v). Notice that the constants v_{ab} are not independent parameters since they were included into the definition of $\mathcal{G}^{\mathrm{in}}_{0,ab}$ and thus they are absorbed by $\kappa^{\mathrm{in}}_{ab}$—see Eqs. (13) and (57). The number of parameters can be reduced if the analyzed system possesses a symmetry which constrains some of the parameters from Eq. (69).

Then for the elastic and inelastic differential rates one finally finds

$$\frac{d\mathrm{Br}^{\mathrm{e}}_\alpha}{dM} = \mathcal{N} \left| \sum_\beta \xi_\beta t_{\beta\alpha} \right|^2 p_3 k_\alpha, \tag{70}$$

$$\frac{d\mathrm{Br}^{\mathrm{in}}_i}{dM} = \mathcal{N} \left| \sum_\alpha \xi_\alpha t_{\alpha i} \right|^2 p_3 k_i^{\mathrm{in}}. \tag{71}$$

In order to arrive at the final expressions various momentum dependencies that are suppressed kinematically in the near-threshold regime were dropped. We confirmed the applicability of those approximations by comparing

[3] In certain cases, however, the Born term can play a crucial role as discussed, e.g., in Ref. [34].

the analytic solution presented above with a solution of the full equations found numerically.

VI. DIRECT INTERACTION IN THE $(\bar{q}Q)(\bar{Q}q)$ SYSTEM

A paradigmatic example of a near-threshold state described by the general formulas derived in the previous section (in fact by their simplified version given by the two-channel Flatté distribution) is the glorious $X(3872)$ charmonium(like) state discovered by the Belle Collaboration in 2003 [21] which resides within less than 1 MeV from the neutral $D\bar{D}^*$ threshold [33]. There exists a vast literature on the description of the X line shapes in its open-charm and hidden-charm decay channels—see, for example, Refs. [9–13,15,35] to mention just a few. We therefore do not dwell on the $X(3872)$ any more and consider another intriguing example of near-threshold phenomena provided by the $Z_b^{(\prime)}$ resonances discovered by the Belle Collaboration in 2011 in the spectrum of bottomoniumlike states [24] and which appear as intermediate states in the $\Upsilon(5S)$ decays [36,37]. Proximity of the observed $Z_b(10610)$ and $Z_b(10650)$ to the $B\bar{B}^*$ and $B^*\bar{B}^*$ thresholds, respectively, hints towards a prominent molecular component of both states [36] and calls for a simultaneous description of the available experimental data for their open- and hidden-bottom decay channels.[4]

A. Contact elastic interaction potential

The four negative-parity heavy-light B mesons have the wave functions

$$B = 0^-_{\bar{b}q}, \qquad \bar{B} = 0^-_{\bar{q}b}, \qquad B^* = 1^-_{\bar{b}q}, \qquad \bar{B}^* = -1^-_{\bar{q}b}, \tag{72}$$

where, for example, the symbol $0^-_{\bar{b}q}$ denotes the quantum numbers $J^P = 0^-$ in the system of antiquark $\bar{b}$ and the light quark q. The charge conjugation operation for a meson $\mathcal{M}$ is defined as

$$\hat{C}\mathcal{M} = \bar{\mathcal{M}}. \tag{73}$$

The direct interaction potential in the elastic channels can be extracted from the effective Lagrangian which describes the $B^{(*)}\bar{B}^{(*)}$ interactions consistent with the heavy-quark spin symmetry (HQSS) [38,39]. Alternatively, if the source of the interaction in the $B^{(*)}\bar{B}^{(*)}$ channels is identified with u-channel quark exchanges then the problem reduces to performing a Fierz transformation from the open-bottom states $(J^-_{\bar{q}b} \otimes J^-_{\bar{b}q})_S$ to the hidden-bottom states $(J^-_{\bar{b}b} \otimes J^-_{\bar{q}q})_S$ [36,37],

$$(0^-_{\bar{q}b} \otimes 0^-_{\bar{b}q})_{S=0} = \frac{1}{2}(0^-_{\bar{b}b} \otimes 0^-_{q\bar{q}})_{S=0} - \frac{\sqrt{3}}{2}(1^-_{\bar{b}b} \otimes 1^-_{\bar{q}q})_{S=0}, \tag{74}$$

$$(1^-_{\bar{q}b} \otimes 1^-_{\bar{b}q})_{S=0} = -\frac{\sqrt{3}}{2}(0^-_{\bar{b}b} \otimes 0^-_{\bar{q}q})_{S=0} - \frac{1}{2}(1^-_{\bar{b}b} \otimes 1^-_{\bar{q}q})_{S=0}, \tag{75}$$

$$(1^-_{\bar{q}b} \otimes 0^-_{\bar{b}q})_{S=1} = \frac{1}{2}(1^-_{\bar{b}b} \otimes 0^-_{\bar{q}q})_{S=1} + \frac{1}{2}(0^-_{\bar{b}b} \otimes 1^-_{\bar{q}q})_{S=1} - \frac{1}{\sqrt{2}}(1^-_{\bar{b}b} \otimes 1^-_{\bar{q}q})_{S=1}, \tag{76}$$

$$(0^-_{\bar{q}b} \otimes 1^-_{\bar{b}q})_{S=1} = \frac{1}{2}(1^-_{\bar{b}b} \otimes 0^-_{\bar{q}q})_{S=1} + \frac{1}{2}(0^-_{\bar{b}b} \otimes 1^-_{\bar{q}q})_{S=1} + \frac{1}{\sqrt{2}}(1^-_{\bar{b}b} \otimes 1^-_{\bar{q}q})_{S=1}, \tag{77}$$

$$(1^-_{\bar{q}b} \otimes 1^-_{\bar{b}q})_{S=1} = -\frac{1}{\sqrt{2}}(1^-_{\bar{b}b} \otimes 0^-_{\bar{q}q})_{S=1} + \frac{1}{\sqrt{2}}(0^-_{\bar{b}b} \otimes 1^-_{\bar{q}q})_{S=1}, \tag{78}$$

$$(1^-_{\bar{q}b} \otimes 1^-_{\bar{b}q})_{S=2} = (1^-_{\bar{b}b} \otimes 1^-_{\bar{q}q})_{S=2}. \tag{79}$$

Since, in the heavy-quark limit, the transition potential in the elastic channels depends only on the light degrees of freedom, then only two parameters (potentials) are needed:

$$V[0^-_{\bar{q}q}] \equiv V_0, \qquad V[1^-_{\bar{q}q}] \equiv V_1. \tag{80}$$

With the help of Eqs. (74)–(79) it is straightforward to find for the transition potentials in various channels:

$$v(0^{++}) = \frac{1}{4}\begin{pmatrix} V_0 + 3V_1 & \sqrt{3}(V_0 - V_1) \\ \sqrt{3}(V_0 - V_1) & 3V_0 + V_1 \end{pmatrix}, \tag{81}$$

$$v(1^{+-}) = \frac{1}{2}\begin{pmatrix} V_0 + V_1 & V_1 - V_0 \\ V_1 - V_0 & V_0 + V_1 \end{pmatrix}, \tag{82}$$

$$v(1^{++}) = {}_{1^{++}}\langle B\bar{B}^*|\hat{V}(1^{++})|B\bar{B}^*\rangle_{1^{++}} = V_1, \tag{83}$$

$$v(2^{++}) = {}_{2^{++}}\langle B^*\bar{B}^*|\hat{V}(2^{++})|B^*\bar{B}^*\rangle_{2^{++}} = V_1, \tag{84}$$

where in Eq. (82) it was used that, according to Eq. (73), the C-odd combinations of the $B^{(*)}$ and B^* mesons are [36,37]

$$|B\bar{B}^*\rangle_{1^{+-}} = \frac{1}{\sqrt{2}}(|B\bar{B}^*\rangle - |\bar{B}B^*\rangle) = -\frac{1}{\sqrt{2}}[(1^-_{\bar{b}b} \otimes 0^-_{\bar{q}q})_{S=1} + (0^-_{\bar{b}b} \otimes 1^-_{\bar{q}q})_{S=1}], \tag{85}$$

[4]It was shown recently that the Z_b states even play a crucial role in understanding the transitions $\Upsilon(3S) \to \Upsilon(1S)\pi\pi$ [25].

$$|B^*\bar{B}^*\rangle_{1^{+-}} = \frac{1}{\sqrt{2}}[(1^-_{\bar{b}b} \otimes 0^-_{\bar{q}q})_{S=1} - (0^-_{\bar{b}b} \otimes 1^-_{\bar{q}q})_{S=1}]. \quad (86)$$

The transition potentials of Eqs. (81)–(84) are equivalent to those obtained in Ref. [39] [Eqs. (18)–(21)]. To recover the latter one is to redefine the contact potentials

$$C_{0a} = \frac{1}{4}V_0 + \frac{3}{4}V_1, \qquad C_{0b} = -\frac{1}{4}V_0 + \frac{1}{4}V_1 \quad (87)$$

and to stick to a different definition of the C-parity used in Ref. [39] that eventually only entails a change of the signs of the off-diagonal terms in the potential $v(0^{++})$.

B. Direct interaction t matrix

For a given momentum-independent direct interaction potential $v_{\alpha\beta}$ the t matrix t^v can be found from Eq. (36),

$$t^v_{\alpha\beta} = v_{\alpha\beta} - \sum_\gamma v_{\alpha\gamma} J_\gamma t^v_{\gamma\beta}, \quad (88)$$

where the loop integrals J_α are defined in Eq. (55) above. The solution of Eq. (88) then reads

$$(t^v)^{-1} = v^{-1} + (R + iI) = v^{-1}_{\rm ren} + iI, \quad (89)$$

where the real part of the loop operator R is absorbed into the renormalization of the contact potential v as

$$v_{\rm ren} = Z^{-1}v, \qquad Z = 1 + vR. \quad (90)$$

Since the direct interaction potential is an input for the model, it is sufficient to stick to its renormalized value from the beginning and therefore the subscript "ren" can be dropped. In addition, this justifies omitting in Eq. (88) all real parts of the loops defined in Eq. (55).

For the channels 1^{++} and 2^{++} Eq. (88) reduces to a single equation $t^v = v - vIt^v$ with the solution

$$t^v = \frac{1}{(2\pi)^2\mu}(\gamma_V + ik)^{-1}, \qquad \gamma_V^{-1} = (2\pi)^2\mu v, \quad (91)$$

where, as was explained above, the real part of the loop integral $J = \int S(\boldsymbol{q})d^3q = R + iI$ is absorbed into the potential v while its imaginary part $(2\pi)^2\mu k$ is retained explicitly. Here μ and k are the reduced mass and the momentum in the corresponding $B^*\bar{B}^{(*)}$ system, respectively.

For the channels 0^{++} and 1^{+-} Eq. (88) turns into a system of two coupled equations with the solution

$$t^v = \frac{1}{\Delta}\begin{pmatrix} v_{11} + \Delta_v J_2 & v_{12} \\ v_{21} & v_{22} + \Delta_v J_1 \end{pmatrix}, \quad (92)$$

where

$$\Delta_v = v_{11}v_{22} - v_{12}v_{21}, \quad (93)$$

$$\Delta = 1 + v_{11}J_1 + v_{22}J_2 + \Delta_v J_1 J_2. \quad (94)$$

As before, the real parts of the loop integrals J_α can be absorbed into a redefinition of the potential $v_{\alpha\beta}$. The quantities μ_α and k_α are the reduced mass and the momentum in the $B^{(*)}\bar{B}^{(*)}$ channel α, respectively. In the nonrelativistic limit

$$k_\alpha(E) = \sqrt{2\mu_\alpha(E - \Delta_\alpha)}\Theta(E - \Delta_\alpha) + i\sqrt{2\mu_\alpha(\Delta_\alpha - E)}\Theta(\Delta_\alpha - E), \quad (95)$$

where Δ_α is the position of the corresponding elastic threshold and the energy is conveniently counted from the lowest of them, $E = M - m_{th}$.

For the quantum numbers 1^{+-}, relevant for the $Z_b^{(\prime)}$'s case [see Eq. (82)],

$$v_{11} = v_{22} = \frac{1}{2}(V_0 + V_1),$$
$$v_{12} = v_{21} = \frac{1}{2}(V_1 - V_0). \quad (96)$$

It is convenient then to introduce parameters γ_s and γ_t such that

$$\gamma_s^{-1} = (2\pi)^2\mu(v_{11} + v_{12}) = (2\pi)^2\mu V_1,$$
$$\gamma_t^{-1} = (2\pi)^2\mu(v_{11} - v_{12}) = (2\pi)^2\mu V_0, \quad (97)$$

where, for simplicity, the difference between the reduced masses in the channels $B\bar{B}^*$ and $B^*\bar{B}^*$ is neglected, so that $\mu_1 = \mu_2 = \mu$.

When expressed in terms of the new parameters γ_s and γ_t, the direct interaction t matrix given by Eq. (92) takes the form

$$t^v = \frac{1}{(2\pi)^2\mu}\frac{1}{\rm Det}\begin{pmatrix} \frac{1}{2}(\gamma_s + \gamma_t) + ik_2 & \frac{1}{2}(\gamma_t - \gamma_s) \\ \frac{1}{2}(\gamma_t - \gamma_s) & \frac{1}{2}(\gamma_s + \gamma_t) + ik_1 \end{pmatrix}, \quad (98)$$

with

$${\rm Det} = \gamma_s\gamma_t - k_1k_2 + \frac{i}{2}(\gamma_s + \gamma_t)(k_1 + k_2). \quad (99)$$

VII. LINE SHAPES OF THE Z_b AND Z_b'

To exemplify the potential of the parametrization derived in this paper we use the latter to describe the line shapes of the $Z_b(10610)$ and $Z_b(10650)$ bottomoniumlike states. For other discussions on the line shapes of the Z_b's, we refer to Refs. [40–42]. We consider the simplest possible version of

the formulas, thus refraining from inclusion of the bare poles that corresponds to setting $v_{a\alpha}(\boldsymbol{p}) = v_{ai}(\boldsymbol{k}) = 0$ and $M_{0.a} \to \infty$ in all formulas above. It should be noticed that inclusion of one or two explicit poles would result in a fit of comparable quality. However, since the data can already be very well described without bare poles, such a fit would not be better and the couplings for the bare states would get little constrained. Thus, at the present stage and given the quality of the data currently available, the bare pole terms are not needed.

The existing experimental data for the Z_b's are exhausted by 7 decay chains:

$$\begin{aligned}
&\Upsilon(5S) \to \pi Z_b^{(\prime)} \to \pi B^{(*)}\bar{B}^*, \\
&\Upsilon(5S) \to \pi Z_b^{(\prime)} \to \pi\pi\Upsilon(nS), \qquad n = 1, 2, 3, \\
&\Upsilon(5S) \to \pi Z_b^{(\prime)} \to \pi\pi h_b(mP), \qquad m = 1, 2.
\end{aligned} \tag{100}$$

Therefore, in the formulas derived above the spectator particle is the pion (particle 3 in Fig. 5) and, with the help of Eqs. (70) and (71), we find for the production rates in two elastic ($B\bar{B}^*$ and $B^*\bar{B}^*$) and five inelastic [$\pi\Upsilon(nS)$ and $\pi h_b(mP)$] channels

$$\begin{aligned}
\frac{d\mathrm{Br}_1^{\mathrm{e}}}{dM} &= \mathcal{N}|t_{11} + \xi t_{21}|^2 p_\pi k_1, \\
\frac{d\mathrm{Br}_2^{\mathrm{e}}}{dM} &= \mathcal{N}|t_{12} + \xi t_{22}|^2 p_\pi k_2, \\
\frac{d\mathrm{Br}_i^{\mathrm{in}}}{dM} &= \mathcal{N}R^2|g_{i1}(t_{11} + \xi t_{21}) + g_{i2}(t_{12} + \xi t_{22})|^2 \\
&\quad \times p_\pi (k_i^{\mathrm{in}})^{2l_i+1},
\end{aligned} \tag{101}$$

respectively, where l_i is the angular momentum in the final state. Analysis of the angular distributions favors the $J^P = 1^+$ assignment for both Z_b states [43]. Since the structures of interest are very close to the $B\bar{B}^*$ and $B^*\bar{B}^*$ thresholds, in the analysis we only take into account the lowest possible orbital angular momenta for the coupled channels, which are the S wave for the $B\bar{B}^*$, $B^*\bar{B}^*$, and $\pi\Upsilon(nS)$ channels and the P wave for the $\pi h_b(mP)$ channels. Therefore, in Eq. (101) above, $l_i = 0$ for the $\pi\Upsilon(nS)$ channels and $l_i = 1$ for the $\pi h_b(mP)$ ones while t_{11}, t_{12}, t_{21}, t_{22} are the components of the 2×2 elastic t matrix $t_{\alpha\beta}$. As was explained above [see Eq. (68)], instead of the original quantities $\mathcal{F}_1$ and $\mathcal{F}_2$ we introduced the overall normalization parameter $\mathcal{N}$ and the ratio ξ and, for simplicity, set $\mu_1 = \mu_2 \equiv \mu$ so that the quantity κ is defined as $R_1 = R_2 \equiv R = (2\pi)^2\mu\kappa$.

Two comments are in order here. First, as was explained before, we neglect the $\pi\pi$ interaction in the final state although it would be needed to ensure exact three-body unitarity. However, since the aim of the suggested approach is to fit the structures in the $\pi\Upsilon(nS)$ and $\pi h_b(mP)$ invariant mass distributions, the cross-channel $\pi\pi$ interaction can only provide a smooth background. In particular, we do not expect the $\pi\pi$ interaction to produce narrow structures in the studied channels. Therefore, while being important when it comes to fitting the two-pion invariant mass distributions in the $\pi\pi\Upsilon(nS)$ channels, the $\pi\pi$ final state interaction is not expected to have any significant impact on the observables discussed in this paper.

The other comment is that, in addition to the three-body pointlike source terms $\Upsilon(5S) \to B^{(*)}\bar{B}^*\pi$ which correspond to the black dot in Fig. 5, the pion emission may proceed from the B-meson lines. Such processes were studied in detail in Ref. [41] and it can be concluded from the results reported there that, at the tree level, the amplitude with such a sequential pion emission is strongly suppressed compared to the three-body pointlike source term. We therefore disregard them here and treat the production mechanism depicted in Fig. 5 as the dominating mechanism.

According to Eq. (98) the direct interaction elastic t matrix t^v is parametrized with 2 parameters γ_s and γ_t and therefore we arrive at the following set of 15 parameters describing the line shapes in 7 elastic and inelastic channels for the Z_b's [see Eq. (100)]

$$\gamma_s, \gamma_t, \kappa, \xi, \mathcal{N}, g_{i\alpha}, \tag{102}$$

where $i = \pi\Upsilon(nS)$, $\pi h_b(mP)$ with $n = 1, 2, 3$, $m = 1, 2$ and $\alpha = B\bar{B}^*$, $B^*\bar{B}^*$.

We perform a simultaneous fit for the background-subtracted and efficiency-corrected distributions in M for the $B^{(*)}\bar{B}^*$ [23,44] and $\pi h_b(mP)$ channels [24]. We cannot fit line shapes in the $\pi\Upsilon(nS)$ channels since they have a significant nonresonant contribution that depends on $M(\pi\pi)$; thus the amplitude analysis has to be multidimensional. Instead, we can predict the $Z_b^{(\prime)}$ line shapes in these channels, as discussed below. Normalizations in different channels are floated independently and we use the measured production cross sections of all seven channels [23,24,44–47] as additional constraints to ensure the correct relative probabilities for the analyzed distributions. The finite experimental resolution is accounted for via a convolution of the resulting distributions with a Gaussian with $\sigma = 6$ MeV. Since κ is practically unconstrained by the fit we fix it to 1 GeV.

As was explained above, the number of parameters can be reduced if some symmetry constraints are applied. In particular, for the system at hand HQSS constraints following from Eqs. (85) and (86) read

$$\frac{g_{[\pi\Upsilon(nS)][B^*\bar{B}^*]}}{g_{[\pi\Upsilon(nS)][B\bar{B}^*]}} = -1, \qquad \frac{g_{[\pi h_b(mP)][B^*\bar{B}^*]}}{g_{[\pi h_b(mP)][B\bar{B}^*]}} = 1, \tag{103}$$

where $n = 1, 2, 3$ and $m = 1, 2$. In addition, as the elastic channels $B\bar{B}^*$ and $B^*\bar{B}^*$ are produced in the decays of the $\Upsilon(5S)$ bottomonium [see Eq. (100)], then the ratio of the sources ξ is subject to the same heavy-quark constraint, that is

TABLE I. Parameters of the model determined from the combined fit to the data for the $\pi h_b(mP)$ final state contained in Ref. [24] and for the $B^{(*)}\bar{B}^*$ final state contained in Ref. [23] (denoted as old data) and in Ref. [44] (denoted as new data).

Fit	Data	γ_s, MeV	γ_t, MeV	ξ	$g_{[\pi h_b(1P)][B^*\bar{B}^*]}/g_{[\pi h_b(1P)][B\bar{B}^*]}$	$g_{[\pi h_b(2P)][B^*\bar{B}^*]}/g_{[\pi h_b(2P)][B\bar{B}^*]}$	C.L.
A	Old	-39 ± 11	-137 ± 29	-1	1	1	32%
B	New	-70^{+32}_{-36}	-83^{+35}_{-38}	-1	1	1	48%
C	New	43^{+37}_{-58}	-211^{+68}_{-58}	-0.80 ± 0.10	$1.8^{+0.9}_{-0.5}$	$1.8^{+0.9}_{-0.5}$	53%

$$\xi = \frac{g_{[\pi\Upsilon(5S)][B^*\bar{B}^*]}}{g_{[\pi\Upsilon(5S)][B\bar{B}^*]}} = -1. \tag{104}$$

We consider three different fits:

Fit A. Combined fit for the data in the $Z_b^{(\prime)} \to \pi h_b(mP)$ $(m = 1, 2)$ channels [24] and for the old data in the $Z_b^{(\prime)} \to B^{(*)}\bar{B}^*$ channels [23] with HQSS constraints (103) and (104) applied.

Fit B. Same as fit A for the new data for the $Z_b^{(\prime)} \to B^{(*)}\bar{B}^*$ channels [44].

Fit C. Same as fit B but with all parameters totally unconstrained.

The parameters of fits A, B, and C are quoted in Table I, from which one can deduce several conclusions. First, the suggested parametrization is obviously able to capture all gross features of the experimental signal and therefore provides a good overall description of the data in all analyzed channels. Second, one is led to conclude that the new data for the $Z_b^{(\prime)} \to B^{(*)}\bar{B}^*$ channels are much more compatible with the HQSS constraints. Indeed, on one hand, the quality of fit B is noticeably better than the quality of fit A. Also, from fits B and C one can see that relaxing the HQSS constraints does not lead to a considerable increase in the quality of the fit. This is to be confronted with the dramatic decrease of the quality of the fit for the old data in the $Z_b^{(\prime)} \to B^{(*)}\bar{B}^*$ channels—from 76% for the totally unconstrained fit from Ref. [19] to 32% for fit A from Table I. Finally, fully unconstrained fit C demonstrates a better agreement with the HQSS constraints (103) and (104) than the similar unconstrained fit to the old data found in Ref. [19].

The line shapes of the $Z_b(10610)$ and $Z_b(10650)$ states in the $B^{(*)}\bar{B}^*$ and $\pi h_b(mP)$ $(m = 1, 2)$ channels are shown in Fig. 6 for all three fits from Table I. In addition, as an example, we show, in Fig. 7, the line shapes in the $\pi\Upsilon(2S)$ channel which come as a prediction of our approach and demonstrate a clear similarity to the experimental data (the last plot in Fig. 7).

Two comments on the fits given in Table I are in order here:

(1) While fits A and B have the HQSS constraints built in, fit C features some HQSS breaking since ξ takes a value different from -1 [see Eq. (104)] and, particularly, since the ratios $g_{[\pi h_b(nP)][B^*\bar{B}^*]}/g_{[\pi h_b(nP)][B\bar{B}^*]}(n = 1, 2)$ deviate from their respective HQSS values (103). This might be because of the complexity of the $\Upsilon(10860)$ state, assigned as the $5S$ bottomonium here, so that the HQSS breaking effects may stem from a mixture of the D-wave bottomonium [48] or non-$\bar{b}b$ components [49] in the $\Upsilon(10860)$ wave function. It is worthwhile noticing that, even in the two-body open-bottom decays of the $\Upsilon(5S)$, the measured branching fractions [33] show a sizable HQSS breaking as well. This was summarized, for example, in Ref. [4]. It is also concluded in Ref. [41] that explicit HQSS breaking operators are needed to describe the Z_b's line shapes in the $\Upsilon(5S) \to \pi B^{(*)}\bar{B}^*$ decays. On the other hand, this deviation may be diminished in the fit to updated experimental data in the future. If, however, the HQSS breaking still persists, one will need to investigate the origin carefully since HQSS is normally very well respected in the bottomonium mass region. In addition to the possible non-S-wave $\bar{b}b$ component for the $\Upsilon(10860)$, the internal dynamics of the Z_b states might be another reason. However, this breaking seems to be rather unlikely to occur due to the reason discussed in Ref. [40] where a large HQSS breaking effect in the ratio $g_{Z_bB\bar{B}^*}/g_{Z_bB^*\bar{B}^*}$ is explained by the proximity of the poles to the corresponding thresholds. Such an effect manifests itself in the pole positions of the amplitude and therefore it was already included in the fits. Furthermore, it was pointed out in Ref. [50] that the S-D mixing effects for the bottom meson pair in the final state of the decay $\Upsilon(5S) \to \pi B^{(*)}\bar{B}^*$ probably only play a minor role for the internal structure of the Z_b states (see also Ref. [51] for a calculation based on the one-meson exchange model).

(2) In fit B which has HQSS built in, the values of γ_s and γ_t are almost the same. It means that the off-diagonal matrix elements of the potential matrix for the interaction between elastic channels almost vanish. Indeed, from Eqs. (96) and (97) and for the parameters of fit B, we have

$$v_{12} = \frac{1}{8\pi^2\mu}(\gamma_s^{-1} - \gamma_t^{-1}) \ll v_{11} = v_{22}. \tag{105}$$

Since $\gamma_s^{-1} \propto V_1$ and $\gamma_t^{-1} \propto V_0$ describe the interaction for the total light-quark spin 1 and 0,

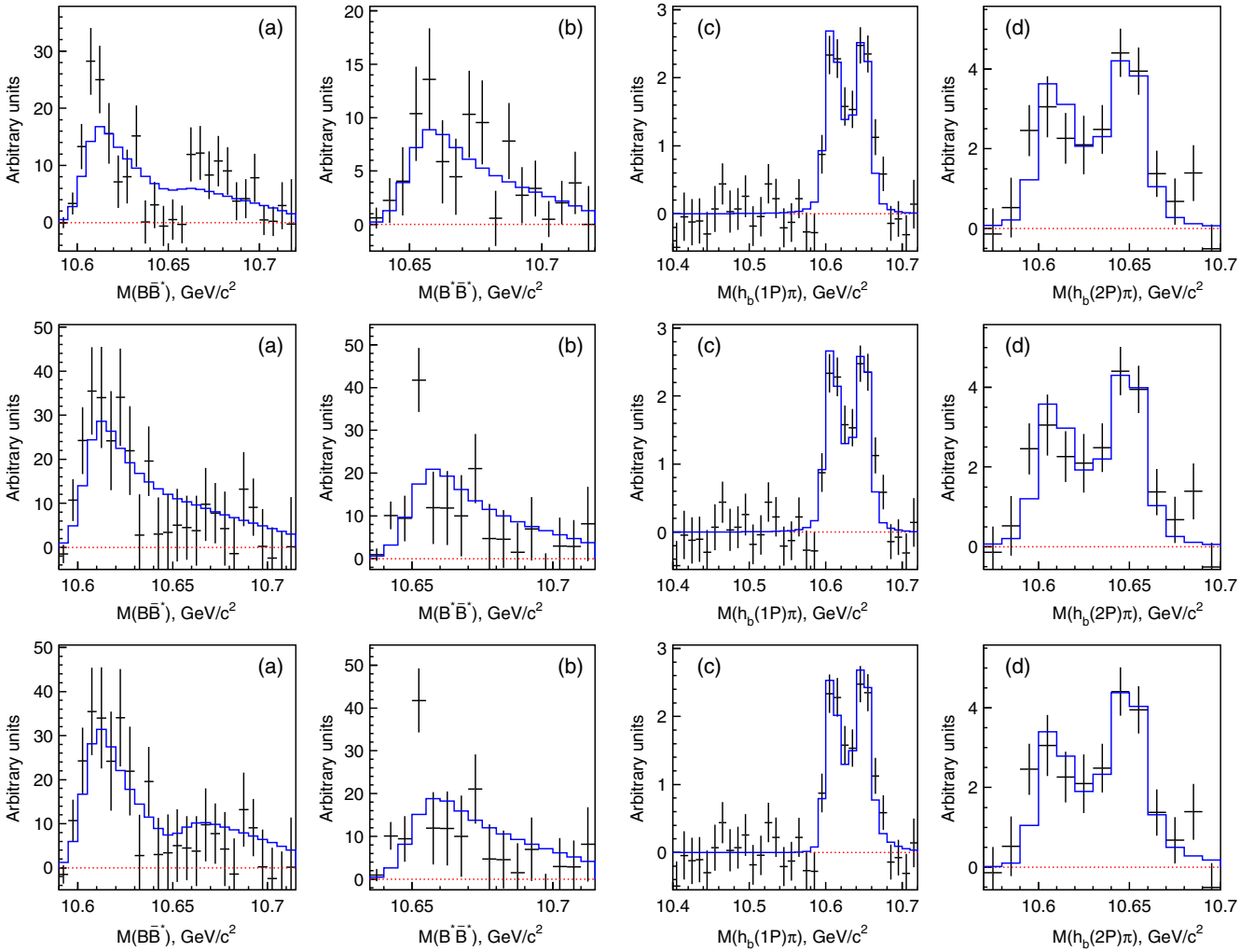

FIG. 6. Fitted line shapes of the $Z_b(10610)$ and $Z_b(10650)$ in the $B^{(*)}\bar{B}^*$ channels [plots (a) and (b)] and in the $\pi h_b(mP)$ $(m = 1, 2)$ channels [plots (c) and (d)]. Parameters of fits A, B, and C are used for the plots in the upper, middle, and lower rows, respectively.

respectively [see Eq. (80)], this is in fact consistent with the observation made recently [52] that the nonobservation of the $Z_b(10650)$ in the $B\bar{B}^*$ invariant mass distribution implies that the interaction between the bottom and antibottom mesons is insensitive to the light quark spin, and thus seems to imply an accidental "light-quark spin symmetry." Indeed, there is little signal of the $Z_b(10650)$ in the plot (a) in the second row of Fig. 6. However, although not prominent, the $Z_b(10650)$ shows up as a bump in the plot (a) in the third row of Fig. 6, which corresponds to fit C with HQSS constraints released. In this fit, γ_s and γ_t do not take similar values any more. This means that the current data require us to understand either the accidental light-quark spin symmetry or a sizable HQSS breaking.

For completeness, we quote all parameters of fit B in Table II.

TABLE II. Parameters of fits B and C. The couplings $g_{[\pi h_b(mP)][B\bar{B}^*]}$ and $g_{[\pi\Upsilon(nS)][B\bar{B}^*]}$ are given in the units of GeV^{-3} and GeV^{-2}, respectively. For both fits, $g_{[\pi\Upsilon(nS)][B^*\bar{B}^*]}/g_{[\pi\Upsilon(nS)][B\bar{B}^*]} = -1$, as required by the HQSS constraints from Eq. (103), while the values of the ratios $g_{[\pi h_b(mP)][B^*\bar{B}^*]}/g_{[\pi h_b(mP)][B\bar{B}^*]}$ can be found in Table I.

Fit	$g_{[\pi h_b(1P)][B\bar{B}^*]}\cdot 10^3$	$g_{[\pi h_b(2P)][B\bar{B}^*]}\cdot 10^3$	$g_{[\pi\Upsilon(1S)][B\bar{B}^*]}\cdot 10^4$	$g_{[\pi\Upsilon(2S)][B\bar{B}^*]}\cdot 10^4$	$g_{[\pi\Upsilon(3S)][B\bar{B}^*]}\cdot 10^4$
B	$2.0^{+0.3}_{-0.2}$	$7.5^{+1.0}_{-0.9}$	1.3 ± 0.3	$5.0^{+0.8}_{-0.9}$	$7.0^{+1.3}_{-1.5}$
C	$1.2^{+0.5}_{-0.4}$	$4.6^{+1.7}_{-1.4}$	1.4 ± 0.3	5.5 ± 1.0	$7.9^{+1.6}_{-1.8}$

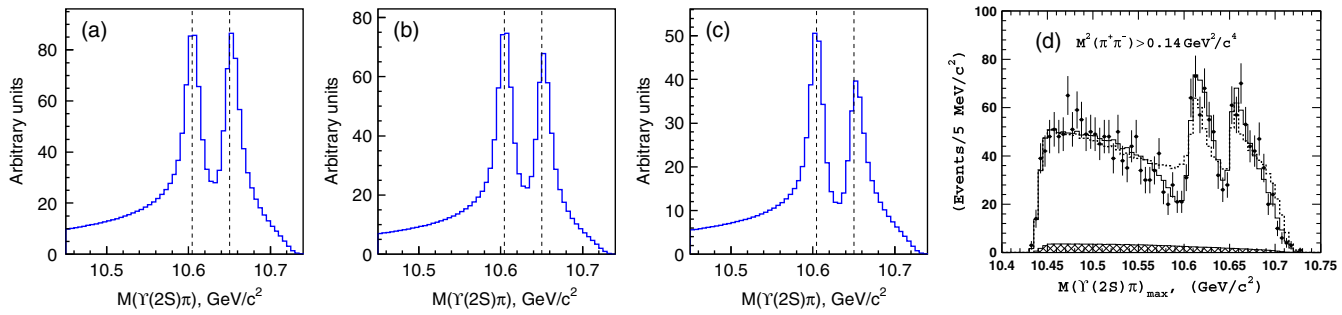

FIG. 7. Plots (a), (b), and (c) are for the predicted line shapes of the $Z_b(10610)$ and $Z_b(10650)$ in the $\pi\Upsilon(2S)$ channel for fits A, B, and C, respectively. To guide the eye, as plot (d), we also show the corresponding experimental figure adapted from Ref. [46]. Notice that the behavior of the line shape below the left shoulder of the lower peak is influenced by the effects which lie beyond the scope of the present paper and will be addressed in future publications. Notice also that the presence of the nonresonant background in the experimental figure does not allow its direct comparison with the predicted line shapes.

VIII. NATURE OF THE $Z_b(10610)$ AND $Z_b(10650)$ FROM DATA

Important information on the nature of the near-threshold states like the $Z_b(10610)$ and $Z_b(10650)$ is encoded in the singularity structure of the amplitudes extracted from the fit,[5] in particular the pole positions and pole residues [53–56]. Therefore we have a closer look at the pole locations of the Z_b states in this section.

The full t matrix considered here has in total seven coupled channels. One might think that the task of searching for the poles of the t matrix is formidable, because the number of Riemann sheets is $2^7 = 128$. However, in practice the problem is as simple as a two-channel one. This is because the thresholds of all the inelastic channels are far away from those of the $B\bar{B}^*$ and $B^*\bar{B}^*$ channels and the interactions among the inelastic channels are very weak and can be safely neglected as it is anyhow done in this paper. Thus any pole which has the potential to produce a measurable effect should reside well above all the inelastic thresholds. Therefore, the relevant Riemann-sheet structure is practically the same as that for the two-channel case.

In order to search for the poles in these relevant Riemann sheets, one needs to put all the inelastic channels in their corresponding unphysical sheets. This is achieved by an analytic continuation with a practical trick of changing the sign of the imaginary part of the inelastic channel Green's functions given in Eqs. (57), (58) and (62).

To study the poles in the two-channel case with the quantum numbers 1^{+-}, it is convenient to make a conformal mapping from the four-Riemann-sheet complex energy plane to the single complex ω plane [57]. For a given energy E, we can write

$$E = \frac{k_1^2}{2\mu} = \frac{k_2^2}{2\mu} + \delta, \tag{106}$$

where $\delta = m_{B^*} - m_B$ denotes the energy gap between the two elastic thresholds. Instead of two complex momenta k_1 and k_2 constrained by the two conditions from Eq. (106), we switch to the complex variable ω, defined via

$$k_1 = \sqrt{\frac{\mu\delta}{2}}\left(\omega + \frac{1}{\omega}\right), \qquad k_2 = \sqrt{\frac{\mu\delta}{2}}\left(\omega - \frac{1}{\omega}\right). \tag{107}$$

This allows us to rewrite the energy as

$$E = \frac{\delta}{4}\left(\omega^2 + \frac{1}{\omega^2} + 2\right). \tag{108}$$

By construction, the complex ω plane is free of unitary cuts.

In the first plot in Fig. 8 we show the mapping of the four Riemann sheets of the complex energy plane, labeled as

$$\begin{aligned} &\text{RS-I:}\ \mathrm{Im}k_1 > 0, && \mathrm{Im}k_2 > 0, \\ &\text{RS-II:}\ \mathrm{Im}k_1 < 0, && \mathrm{Im}k_2 > 0, \\ &\text{RS-III:}\ \mathrm{Im}k_1 > 0, && \mathrm{Im}k_2 < 0, \\ &\text{RS-IV:}\ \mathrm{Im}k_1 < 0, && \mathrm{Im}k_2 < 0, \end{aligned} \tag{109}$$

onto the ω complex plane. The thick solid line corresponds to real values of the energy E on the first sheet, and the part of the imaginary ω axis with $\mathrm{Im}\omega > 1$ corresponds to negative values of E, thus representing energies below the $B\bar{B}^*$ threshold.

It is easy to see from Eq. (107) that the $B\bar{B}^*$ threshold ($k_1 = 0$) appears at $\omega = \pm i$ and the $B^*\bar{B}^*$ ($k_2 = 0$) threshold appears at $\omega = \pm 1$. Thus the near-threshold regions correspond to the vicinities of $|\omega| = 1$. To be able to distinguish between the poles according to their relevance for producing structures in the amplitude in the physical region, it is worthwhile to discuss the structure of the

[5]It has to be noticed that the obtained values of the parameters cannot be compared directly with those from, e.g., Ref. [39] since, in the latter paper, a Gaussian vertex form factor was used to regularize the Lippmann-Schwinger equation and the contact terms are scale dependent.

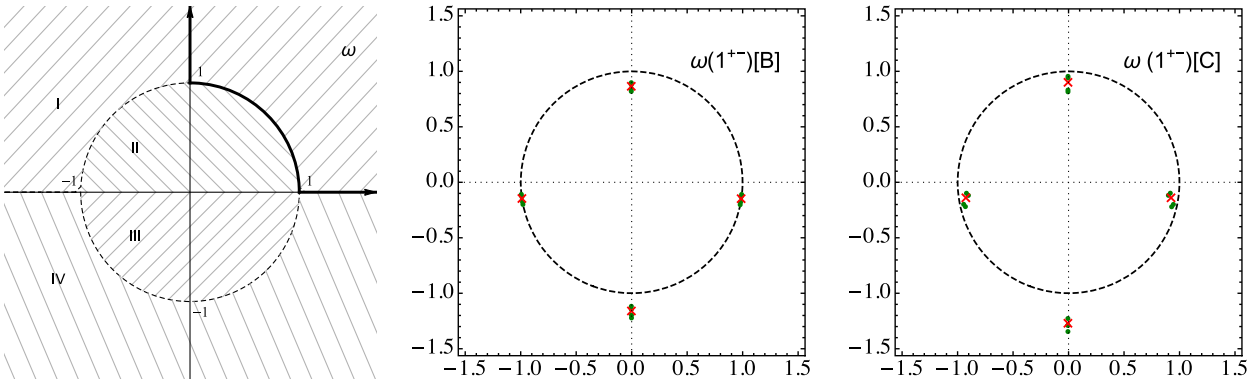

FIG. 8. First plot: Four Riemann sheets mapped into the ω plane. The thick solid line corresponds to the real axis in the first Riemann sheet of the complex energy plane. Second plot: The poles of the full t matrix which correspond to the quantum numbers 1^{+-} and to the set of parameters from fit B—see Table I. The red crosses mark the central values and the green dots show the upper and the lower bounds due to the uncertainties in the fitted parameters. Third plot: The same as in the second plot but for the set of parameters from fit C.

Riemann sheets in some more detail. In particular, between the thresholds, RS-I is glued with RS-II and RS-III is glued with RS-IV along the real energy axis, since crossing this axis changes the sign of Im k_1. Above the higher threshold, crossing the real energy axis changes the signs of both Im k_1 and Im k_2 so that, in this region, RS-I is attached to RS-IV and RS-II is attached to RS-III.

We find that the 1^{+-} t matrix possesses four poles in the complex ω plane, shown in Fig. 8. The pole near the imaginary axis in the lower half ω plane corresponds to a pole below the $B\bar{B}^*$ threshold lying on RS-IV of the complex energy plane. It therefore appears far away from the physical region and has little impact on the physical amplitude. It will not be discussed below.

The pole in the upper half ω plane (if we switch off the inelastic channels, it is located exactly on the imaginary axis) lies nearly on the real axis on RS-II of the complex energy plane, so it describes a virtual state. It is close to the $B\bar{B}^*$ threshold and corresponds to the $Z_b(10610)$. The nonzero real part of the pole location in the ω-plane (which translates into a finite imaginary part in the energy plane) reflects the fact that the $Z_b(10610)$ can decay into the inelastic channels. Notice that, for the parameters from fit C, $v_{11} \propto \gamma_s^{-1} + \gamma_t^{-1} > 0$ and therefore, in the single-channel case (neglecting the $B^*\bar{B}^*$ channel), the t matrix

$$t \propto \frac{1}{v_{11}^{-1} + i(2\pi)^2 \mu k_1} \tag{110}$$

would have a bound-state pole. However, in the two-channel case, the pole in the vicinity of the $B\bar{B}^*$ threshold is a virtual state. This means the $B^*\bar{B}^*$ channel effectively reduces the attraction in the $B\bar{B}^*$ system and turns the bound state into a virtual state. For the parameters from fit B the $Z_b(10610)$ pole corresponds to a virtual state both in the single-channel and two-channel case.

The other two poles, with $\omega \simeq \pm 1$, are a pair of conjugated poles below the $B^*\bar{B}^*$ threshold. We focus on the right one, for it is this pole that is closest to the physical region. This pole lies on RS-IV (RS-III) for fit B (C) and corresponds to the $Z_b(10650)$. The nonzero imaginary part of the pole reflects the fact that $Z_b(10650)$ can decay into the lower $B\bar{B}^*$ channel as well as into the inelastic channels. This pole is very close to the $B^*\bar{B}^*$ threshold and as such it is able to produce a pronounced peak in the line shape. For fit C, the path from the pole in RS-III to the physical RS-I is to go up to the $B^*\bar{B}^*$ threshold, to enter RS-II and then to approach RS-I from below the $B^*\bar{B}^*$ threshold—see the sketch in Fig. 9 (or to go to RS-IV from below the $B^*\bar{B}^*$ threshold and then approach RS-I from above that threshold). For fit B the pole appears on RS-IV and therefore it has a simpler path to the physical region by crossing the cut above the $B^*\bar{B}^*$ threshold since RS-I and RS-IV are directly glued there.

The Z_b and Z_b' energies relative to the respective thresholds,

$$\begin{aligned} \varepsilon_B(Z_b) &\equiv M(B\bar{B}^*) - M(Z_b), \\ \varepsilon_B(Z_b') &\equiv M(B^*\bar{B}^*) - M(Z_b'), \end{aligned} \tag{111}$$

are

$$\begin{aligned} \varepsilon_B(Z_b) &= (1.10^{+0.79}_{-0.54} \pm i0.06^{+0.02}_{-0.02})\ \text{MeV}, \\ \varepsilon_B(Z_b') &= (1.10^{+0.79}_{-0.53} \pm i0.08^{+0.03}_{-0.05})\ \text{MeV}, \end{aligned} \tag{112}$$

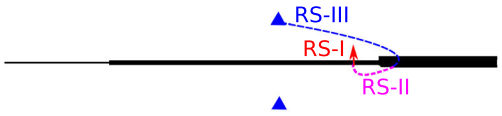

FIG. 9. The path of the RS-III pole to RS-I. The complex conjugated pole is also shown but not its path.

for the parameters from fit B, and

$$\varepsilon_B(Z_b) = (0.60^{+1.40}_{-0.49} \pm i0.02^{+0.02}_{-0.01})\ \text{MeV},$$
$$\varepsilon_B(Z_b') = (0.97^{+1.42}_{-0.68} \pm i0.84^{+0.22}_{-0.34})\ \text{MeV}, \quad (113)$$

for the parameters from fit C. In order to determine the uncertainties of the pole positions we varied the parameters γ_s and γ_t within their ranges allowed by the respective fit. We notice that the real parts of the poles are always below the corresponding thresholds. In addition, the close similarity of the two pole positions for fit B is again a consequence of nearly vanishing v_{12}—see the discussion around Eq. (105).

As one can see, the current data are consistent with both $Z_b(10610)$ and $Z_b(10650)$ as virtual states. This may have severe implications for the interpretation of their nature, since only states with a dominant two-hadron component can be virtual states.[6] Thus our findings give a strong support to the conjecture that the two Z_b states qualify as hadronic molecules. Meanwhile, improved data are necessary to confirm this conclusion.

In the remainder of this section we demonstrate how well the pole locations are determined by the data currently available. To proceed in this direction we stick to the $Z_b(10610)$ pole and consider fits B and C. We observe that the parameters of the fits do not change appreciably, if only the direct interaction t matrix t^v is retained in the elastic t matrix. We also notice that, in the current data set, the influence of the inelastic channels on the line shapes is not very strong either, their role being mainly to provide a finite imaginary part to the poles. We therefore now study the poles of just the direct interaction t matrix, t^v, which depends only on γ_s and γ_t. In the (γ_s, γ_t)-plane we identify various regions, which correspond to different Riemann sheets—see Fig. 10. The actual values of the parameters γ_s and γ_t taken from fits B and C are shown by the black dots with the error bars. The red curve

$$\gamma_t = (\gamma_s^{-1} - \sqrt{2/(\mu\delta)})^{-1} \quad (114)$$

separates the parameter space for the $Z_b(10610)$ as a virtual state from that for the $Z_b(10610)$ as a bound state. Then each blue (green) curve corresponds to a bound (virtual) state with the pole energy, relative to the $B\bar{B}^*$ threshold, quoted explicitly, in MeV, near every curve.

From Fig. 10 one can see that, while the data are rather uncertain and the parameters γ_s and γ_t found from different fits differ substantially, the corresponding dots in the (γ_s, γ_t)-plane nevertheless reside in the "green" domain (virtual state) sufficiently far away from the red boundary curve. Therefore, the conclusion that the $Z_b(10610)$ is a virtual state can be treated as a robust prediction from the data. A similar conclusion holds concerning the nature of the $Z_b(10650)$ as a resonance; however, even in the absence of the inelastic channels, the $Z_b(10650)$ pole has an imaginary part and therefore its fate cannot be demonstrated in a plot as simple as that for the $Z_b(10610)$ given in Fig. 10.

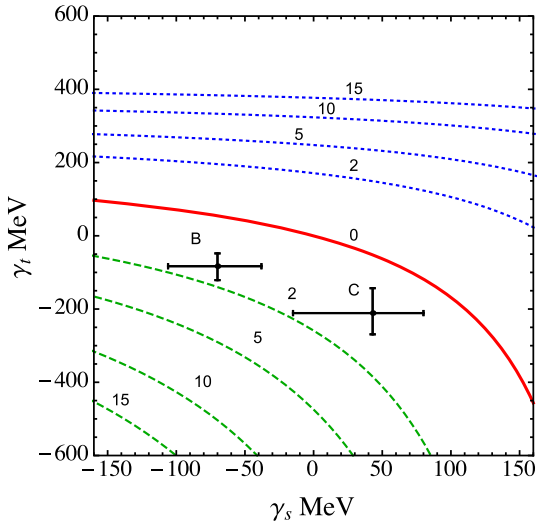

FIG. 10. The space of parameters (γ_t versus γ_s) for the poles of t^v in the channel 1^{+-} close to the $B\bar{B}^*$ threshold [$Z_b(10610)$ state]. The blue and green curves correspond to different Riemann sheets (RS-I versus RS-II, respectively) and the red line gives the boundary between the two regions. The energy of the state relative to the threshold is quoted, in MeV, at every curve. The black dots with the error bars show the actual values of the parameters γ_s and γ_t for fits B and C taken from Table I.

IX. REMARKS ON THE POSSIBLE ROLE OF PION EXCHANGES

The role of one-pion exchange (OPE) on the formation of exotic resonances and, in particular, of hadronic molecules is discussed heavily in the literature. While Refs. [39,58,59] argue that this contribution to the potential is perturbative, Refs. [60,61] claim it to be a crucial contribution to the binding of the two-hadron system.

It was stressed in Ref. [62] that from the point of view of field theoretical consistency the significance of the OPE for the binding energy of the charmonium state $X(3872)$ cannot be defined unambiguously. Given an apparent similarity of the pion exchanges between $D^{(*)}$ mesons and $B^{(*)}$ mesons, the same conclusion holds for the Z_b's. Meanwhile, the long-range tail of the OPE potential might distort the Z_b's line shapes significantly [63]. In addition, it might also induce a significant mixing between the $B\bar{B}^*$ and $B^*\bar{B}^*$ channels as observed in Ref. [52]. We therefore briefly comment on the possible role of the OPE here—a detailed calculation including pion exchanges will be presented in a subsequent publication [64].

[6]By solving the Schrödinger equation for a four-quark system, tetraquark states correspond to the bound states of four quarks and thus cannot be virtual states.

Clearly, the leading effects that determine the line shapes are the pole positions of the two Z_b resonances. In the analysis of the existing data presented above the pole locations emerged from a subtle interplay of the channel couplings. We expect this pattern to persist also when pion exchanges are included, since still free parameters can be adjusted to locate the poles to where data request them to be. Effectively this means that, compared to this analysis, the pion exchange can at most slightly vary the Z_b line shapes. In particular, we do not expect this effect to be as large as announced in Ref. [63] for two reasons: first of all, the analysis of this work did not consider the effect of the interplay of the two poles (determined by their location in the complex plane) on the experimental signals and, secondly, the effect of the OPE was maximized in Ref. [63] by using an effective pion mass $\mu_\pi = \sqrt{m_\pi^2 - \delta^2}$, with $\delta = m_{B^*} - m_B$, in the expression for the static OPE. However, this kind of OPE is correct only for the on-shell potential in the $B\bar{B}^*$ channel and takes a different structure in the $B^*\bar{B}^*$ channel as well as for the transition potential. In addition, the (half-)off-shell potential, relevant here, is energy dependent and when spanning an energy range that covers both Z_b states and keeping effects of the order of δ, also the energy dependence of the OPE potential needs to be kept, which is of the same order. This changes the effective pion mass in a nontrivial way over the relevant energy range. It is also important to keep in mind that as soon as the energy dependence of the pion exchange contribution is to be kept, the recoil terms of the B mesons need to be kept as well, for they contribute to the same order, as stressed in Ref. [65] in a different context. Similar arguments as the ones just presented also allow one to question the claim of Ref. [52] that the contribution of the OPE spoils the light quark spin symmetry. More details will be given elsewhere [64].

Therefore, to summarize the arguments just presented, we expect that even if OPE were included in the analysis of the data for the Z_b states the line shapes would change only slightly. It should be stressed that regardless of this claim a systematic study of the pion exchange contribution to exotic states is still very valuable. For example, the quark mass dependence of exotic states can only be studied in a controlled way with this contribution included [66–68]. This is of relevance for chiral extrapolations of lattice data that at present exist only at unphysically high quark masses [69]. Another example of the relevance of the OPE for studies of exotic states is given in Ref. [70], where it is pointed out that it leads to a very specific pattern of exotic states with respect to their quantum numbers.

X. SUMMARY

In this paper we formulate and analytically solve a coupled-channel problem for the scattering t matrix involving elementary states and a set of elastic and inelastic channels coupled to each other. The solution found can be viewed as a further generalization of the approach presented before in Refs. [8,16]. It should be stressed that since the approach is based on the Lippmann-Schwinger equations for the coupled-channel problem, all unitarity and analyticity constraints for the t matrix are fulfilled automatically. In particular, in contrast to earlier works, the inelastic channels are taken into account nonperturbatively; that is they are iterated to all orders. Then unitarity guarantees that all imaginary parts are included in a self-consistent way. On the other hand, since to leading order in a low-energy expansion there is no direct interaction within the inelastic channels, at least for the type of the systems discussed here, the inelastic channels enter the expressions only additively. As a result it is very easy to include additional inelastic channels.

We present a parametrization of the solution of the equations which appears to be relatively simple but should be powerful enough to describe line shapes of near-threshold states in a wide class of reactions. As a byproduct of the explicit unitarity of the approach, the suggested parametrization allows one to test the existing experimental data for completeness. Indeed, if there exist not yet measured inelastic channels coupled to the elastic ones, the former will contribute to the inelasticities (57) and (58). The corresponding contributions would induce additional imaginary parts of the effective potentials, not linked to the decays known experimentally. If the best fit to all existing data gives negligibly small values of these additional inelasticities, the model can be regarded as complete up to the precision of the experimental data. On the contrary, large values of the additional imaginary parts would indicate a large violation of unitarity which can only be recovered by enlarging the basis of the channels explicitly included in the model. This would also mean that additional experimental efforts are necessary to identify and to measure the missing inelastic channels.

Finally, we exemplify the suggested approach by the line shapes for the bottomoniumlike states Z_b and Z_b'. Without introducing any elementary state, the experimental data for the Z_b and Z_b' can be described well, and poles corresponding to these two states with $J^{PC} = 1^{+-}$ and $I = 1$ are found in the t matrix. We conclude that the $Z_b(10610)$ is a virtual state located on the second Riemann sheet near the $B\bar{B}^*$ threshold while the $Z_b(10650)$ is a resonance on the third or fourth Riemann sheet (however very close to the first Riemann sheet) lying near the $B^*\bar{B}^*$ threshold.

With the parameters extracted from the combined fit for the data, pole positions can be predicted in the complementary channels, with the quantum numbers 0^{++}, 1^{++}, and 2^{++}, in addition to those which have the quantum numbers 1^{+-} and correspond to the $Z_b(10610)$ and $Z_b(10650)$ states. The presence of such additional isovector poles complies very well with the expectations of the existence of more isovector hidden-bottom hadronic molecules, called W_b—see Refs. [37,71]. However we refrain

from further dwelling on the W_b's here because their study requires some caution and, in particular, might call for the inclusion of the pion exchanges. We therefore leave this for future publications.

Unfortunately, with the present quality of the data, the parameters extracted from the fits are very uncertain (notice, for example, the opposite signs of the parameter γ_s in fits B and C as well as a factor 3 difference in γ_l, while both fits provide a similar good overall description of the data) and so are the predictions for the pole positions found with the help of these parameters. It is expected however that future high statistics and high resolution experiments should provide more accurate and more complete data sets.

Finally, we argue that the contribution of the nonseparable one-pion exchange potential is small, once the parameters are refitted with pion exchanges included. As a result, it should be safe to apply the parametrization scheme presented here also to further experimental analyses. In particular, the use of sums of Breit-Wigner functions should be abandoned for the analysis of near-threshold states.

ACKNOWLEDGMENTS

We would like to thank Alexander Bondar, Martin Cleven, Johann Haidenbauer and Andreas Nogga for valuable discussions. This work is supported in part by the DFG and the NSFC through funds provided to the Sino-German CRC 110 "Symmetries and the Emergence of Structure in QCD" (NSFC Grant No. 11261130311). R. M. and A. N. acknowledge support from the Russian Science Foundation (Grant No. 15-12-30014). F.-K. G. is partially supported by the Thousand Talents Plan for Young Professionals.

[1] N. Brambilla *et al.*, Heavy quarkonium: Progress, puzzles, and opportunities, Eur. Phys. J. C **71**, 1534 (2011).
[2] N. Brambilla *et al.*, QCD and strongly coupled gauge theories: Challenges and perspectives, Eur. Phys. J. C **74**, 2981 (2014).
[3] T. Abe *et al.* (Belle-II Collaboration), Belle II technical design report, arXiv:1011.0352.
[4] A. G. Drutskoy, F.-K. Guo, F. J. Llanes-Estrada, A. V. Nefediev, and J. M. Torres-Rincon, Hadron physics potential of future high-luminosity B-factories at the $\Upsilon(5S)$ and above, Eur. Phys. J. A **49**, 7 (2013).
[5] D. M. Asner *et al.*, Physics at BES-III, Int. J. Mod. Phys. A **24**, S1-794 (2009).
[6] M. F. M. Lutz *et al.* (PANDA Collaboration), Physics performance report for PANDA: Strong interaction studies with antiprotons, arXiv:0903.3905.
[7] S. M. Flatte, Coupled-channel analysis of the $\pi\eta$ and $K\bar{K}$ systems near $K\bar{K}$ threshold, Phys. Lett. **63B**, 224 (1976).
[8] V. Baru, C. Hanhart, Y. S. Kalashnikova, A. E. Kudryavtsev, and A. V. Nefediev, Interplay of quark and meson degrees of freedom in a near-threshold resonance, Eur. Phys. J. A **44**, 93 (2010).
[9] C. Hanhart, Yu. S. Kalashnikova, A. E. Kudryavtsev, and A. V. Nefediev, Reconciling the $X(3872)$ with the near-threshold enhancement in the $D^0\bar{D}^{*0}$ final state, Phys. Rev. D **76**, 034007 (2007).
[10] Y. S. Kalashnikova and A. V. Nefediev, Nature of $X(3872)$ from data, Phys. Rev. D **80**, 074004 (2009).
[11] Y. S. Kalashnikova, A. E. Kudryavtsev, and A. V. Nefediev, Quark and meson degrees of freedom in the $X(3872)$ charmonium, Phys. At. Nucl. **73**, 1592 (2010).
[12] E. Braaten and M. Lu, Line shapes of the $X(3872)$, Phys. Rev. D **76**, 094028 (2007).
[13] E. Braaten and J. Stapleton, Analysis of $J/\psi\pi^+\pi^-$ and $D^0\bar{D}^0\pi^0$ decays of the $X(3872)$, Phys. Rev. D **81**, 014019 (2010).
[14] O. Zhang, C. Meng, and H. Q. Zheng, Ambiversion of $X(3872)$, Phys. Lett. B **680**, 453 (2009).
[15] P. Artoisenet, E. Braaten, and D. Kang, Using line shapes to discriminate between binding mechanisms for the $X(3872)$, Phys. Rev. D **82**, 014013 (2010).
[16] C. Hanhart, Y. S. Kalashnikova, and A. V. Nefediev, Interplay of quark and meson degrees of freedom in a near-threshold resonance: Multi-channel case, Eur. Phys. J. A **47**, 101 (2011).
[17] C. Hanhart, Y. S. Kalashnikova, and A. V. Nefediev, Lineshapes for composite particles with unstable constituents, Phys. Rev. D **81**, 094028 (2010).
[18] C. Meng, J. J. Sanz-Cillero, M. Shi, D. L. Yao, and H. Q. Zheng, Refined analysis on the $X(3872)$ resonance, Phys. Rev. D **92**, 034020 (2015).
[19] C. Hanhart, Y. S. Kalashnikova, P. Matuschek, R. V. Mizuk, A. V. Nefediev, and Q. Wang, Practical Parametrization for Line Shapes of Near-Threshold States, Phys. Rev. Lett. **115**, 202001 (2015).
[20] G. Gokhroo *et al.* (Belle Collaboration), Observation of a Near-Threshold $D^0\bar{D}^0\pi^0$ Enhancement in $B \to D^0\bar{D}^0\pi^0 K$ Decay, Phys. Rev. Lett. **97**, 162002 (2006).
[21] S. K. Choi *et al.* (Belle Collaboration), Observation of a Narrow Charmoniumlike State in Exclusive $B^\pm \to K^\pm\pi^+\pi^- J/\psi$ Decays, Phys. Rev. Lett. **91**, 262001 (2003).
[22] P. del Amo Sanchez *et al.* (*BABAR* Collaboration), Evidence for the decay $X(3872) \to J/\psi\omega$, Phys. Rev. D **82**, 011101 (2010).
[23] I. Adachi *et al.* (Belle Collaboration), Study of three-body Y (10860) decays, arXiv:1209.6450.
[24] A. Bondar *et al.* (Belle Collaboration), Observation of Two Charged Bottomoniumlike Resonances in $\Upsilon(5S)$ Decays, Phys. Rev. Lett. **108**, 122001 (2012).
[25] Y. H. Chen, J. T. Daub, F. K. Guo, B. Kubis, U.-G. Meißner, and B. S. Zou, Effect of Z_b states on $\Upsilon(3S) \to \Upsilon(1S)\pi\pi$ decays, Phys. Rev. D **93**, 034030 (2016).

[26] I. V. Danilkin, V. D. Orlovsky, and Y. A. Simonov, Hadron interaction with heavy quarkonia, Phys. Rev. D **85**, 034012 (2012).

[27] I. V. Danilkin and Y. A. Simonov, Channel coupling in heavy quarkonia: Energy levels, mixing, widths and new states, Phys. Rev. D **81**, 074027 (2010).

[28] X.-H. Liu, F.-K. Guo, and E. Epelbaum, Extracting $\pi\pi S$-wave scattering lengths from cusp effect in heavy quarkonium dipion transitions, Eur. Phys. J. C **73**, 2284 (2013).

[29] L. Liu, H. W. Lin, and K. Orginos, Charmed hadron interactions, *Proc. Sci.*, LATTICE2008 (2008) 112.

[30] W. Detmold, S. Meinel, and Z. Shi, Quarkonium at nonzero isospin density, Phys. Rev. D **87**, 094504 (2013).

[31] K. Nakano, Two potential formalisms and the Coulomb-nuclear interference, Phys. Rev. C **26**, 1123 (1982).

[32] C. Hanhart, A new parameterization for the pion vector form factor, Phys. Lett. B **715**, 170 (2012).

[33] K. A. Olive *et al.* (Particle Data Group Collaboration), Review of particle physics, Chin. Phys. C **38**, 090001 (2014).

[34] F.-K. Guo, C. Hanhart, Q. Wang, and Q. Zhao, Could the near-threshold XYZ states be simply kinematic effects?, Phys. Rev. D **91**, 051504 (2015).

[35] I. V. Danilkin and Y. A. Simonov, Dynamical Origin and the Pole Structure of $X(3872)$, Phys. Rev. Lett. **105**, 102002 (2010).

[36] A. E. Bondar, A. Garmash, A. I. Milstein, R. Mizuk, and M. B. Voloshin, Heavy quark spin structure in Z_b resonances, Phys. Rev. D **84**, 054010 (2011).

[37] M. B. Voloshin, Radiative transitions from $\Upsilon(5S)$ to molecular bottomonium, Phys. Rev. D **84**, 031502 (2011).

[38] M. T. AlFiky, F. Gabbiani, and A. A. Petrov, $X(3872)$: Hadronic molecules in effective field theory, Phys. Lett. B **640**, 238 (2006).

[39] J. Nieves and M. P. Valderrama, The heavy quark spin symmetry partners of the $X(3872)$, Phys. Rev. D **86**, 056004 (2012).

[40] M. Cleven, F.-K. Guo, C. Hanhart, and U.-G. Meißner, Bound state nature of the exotic Z_b states, Eur. Phys. J. A **47**, 120 (2011).

[41] T. Mehen and J. W. Powell, Line shapes in $\Upsilon(5S) \to B^{(*)}\bar{B}^{(*)}\pi$ with $Z(10610)$ and $Z(10650)$ using effective field theory, Phys. Rev. D **88**, 034017 (2013).

[42] W. S. Huo and G. Y. Chen, The nature of the Z_b states from a combined analysis of $\Upsilon(5S) \to h_b(mP)\pi^+\pi^-$ and $\Upsilon(5S) \to B^{(*)}\bar{B}^{(*)}\pi$, Eur. Phys. J. C **76**, 172 (2016).

[43] I. Adachi (Belle Collaboration), Observation of two charged bottomonium-like resonances, arXiv:1105.4583.

[44] A. Garmash *et al.* (Belle Collaboration), Study of $e^+e^- \to B^{(*)}\bar{B}^{(*)}\pi^\pm$ at $\sqrt{s} = 10.866$ GeV, arXiv:1512.07419.

[45] I. Adachi *et al.* (Belle Collaboration), First Observation of the P-wave Spin-Singlet Bottomonium States $h_b(1P)$ and $h_b(2P)$, Phys. Rev. Lett. **108**, 032001 (2012).

[46] A. Garmash *et al.* (Belle Collaboration), Amplitude analysis of $e^+e^- \to \Upsilon(nS)\pi^+\pi^-$ at $\sqrt{s} = 10.865$ GeV, Phys. Rev. D **91**, 072003 (2015).

[47] A. Abdesselam *et al.* (Belle Collaboration), Energy scan of the $e^+e^- \to h_b(nP)\pi^+\pi^-$ $(n = 1, 2)$ cross sections and evidence for the $\Upsilon(11020)$ decays into charged bottomonium-like states, arXiv:1508.06562.

[48] F.-K. Guo, U.-G. Meißner, and C.-P. Shen, Enhanced breaking of heavy quark spin symmetry, Phys. Lett. B **738**, 172 (2014).

[49] A. Ali, C. Hambrock, and M. J. Aslam, Tetraquark Interpretation of the BELLE Data on the Anomalous $\Upsilon(1S)\pi^+\pi^-$ and $\Upsilon(2S)\pi^+\pi^-$ Production near the $\Upsilon(5S)$ Resonance, Phys. Rev. Lett. **104**, 162001 (2010); **107**, 049903 (2011).

[50] M. B. Voloshin, Enhanced mixing of partial waves near threshold for heavy meson pairs and properties of $Z_b(10610)$ and $Z_b(10650)$ resonances, Phys. Rev. D **87**, 074011 (2013).

[51] Z. F. Sun, J. He, X. Liu, Z. G. Luo, and S. L. Zhu, $Z_b(10610)^\pm$ and $Z_b(10650)^\pm$ as the $B^*\bar{B}$ and $B^*\bar{B}^*$ molecular states, Phys. Rev. D **84**, 054002 (2011).

[52] M. B. Voloshin, Light quark spin symmetry in Z_b resonances?, arXiv:1601.02540.

[53] S. Weinberg, Elementary particle theory of composite particles, Phys. Rev. **130**, 776 (1963).

[54] V. Baru, J. Haidenbauer, C. Hanhart, Yu. S. Kalashnikova, and A. E. Kudryavtsev, Evidence that the $a_0(980)$ and $f_0(980)$ are not elementary particles, Phys. Lett. B **586**, 53 (2004).

[55] F. Aceti and E. Oset, Wave functions of composite hadron states and relationship to couplings of scattering amplitudes for general partial waves, Phys. Rev. D **86**, 014012 (2012).

[56] H. Nagahiro and A. Hosaka, Elementarity of composite systems, Phys. Rev. C **90**, 065201 (2014).

[57] M. Kato, Analytical properties of two-channel S-matrix, Ann. Phys. (N.Y.) **31**, 130 (1965).

[58] S. Fleming, M. Kusunoki, T. Mehen, and U. van Kolck, Pion interactions in the $X(3872)$, Phys. Rev. D **76**, 034006 (2007).

[59] J. Nieves and M. P. Valderrama, Deriving the existence of $B\bar{B}^*$ bound states from the $X(3872)$ and heavy quark symmetry, Phys. Rev. D **84**, 056015 (2011).

[60] N. A. Tornqvist, Possible Large Deuteron-Like Meson Meson States Bound by Pions, Phys. Rev. Lett. **67**, 556 (1991).

[61] E. S. Swanson, Short range structure in the $X(3872)$, Phys. Lett. B **588**, 189 (2004).

[62] V. Baru, E. Epelbaum, A. A. Filin, F.-K. Guo, H.-W. Hammer, C. Hanhart, U.-G. Meißner, and A. V. Nefediev, Remarks on study of $X(3872)$ from effective field theory with pion-exchange interaction, Phys. Rev. D **91**, 034002 (2015).

[63] M. B. Voloshin, Modification by pion exchange of near threshold resonance line shape in open heavy flavour channel, Phys. Rev. D **92**, 114003 (2015).

[64] J.-L. Wynen *et al.* (to be published).

[65] C. Hanhart and A. Wirzba, Remarks on $NN \to NN\pi$ beyond leading order, Phys. Lett. B **650**, 354 (2007).

[66] V. Baru, E. Epelbaum, A. A. Filin, C. Hanhart, U.-G. Meißner, and A. V. Nefediev, Quark mass dependence of the $X(3872)$ binding energy, Phys. Lett. B **726**, 537 (2013).

[67] M. Jansen, H.-W. Hammer, and Y. Jia, Light quark mass dependence of the $X(3872)$ in an effective field theory, Phys. Rev. D **89**, 014033 (2014).

[68] V. Baru, E. Epelbaum, A. A. Filin, J. Gegelia, and A. V. Nefediev, Binding energy of the $X(3872)$ at unphysical pion masses, Phys. Rev. D **92**, 114016 (2015).

[69] S. Prelovsek and L. Leskovec, Evidence for $X(3872)$ from DD^* Scattering on the Lattice, Phys. Rev. Lett. **111**, 192001 (2013).

[70] M. Cleven, F.-K. Guo, C. Hanhart, Q. Wang, and Q. Zhao, Employing spin symmetry to disentangle different models for the XYZ states, Phys. Rev. D **92**, 014005 (2015).

[71] T. Mehen and J. W. Powell, Heavy quark symmetry predictions for weakly bound B-meson molecules, Phys. Rev. D **84**, 114013 (2011).